Title

The funny current If is essential for the fight-or-flight response in cardiac pacemaker cells

Journal

The Journal of General Physiology, 154(12)

ISSN

0022-1295

Authors

Peters, Colin H
Rickert, Christian
Morotti, Stefano
et al.

Publication Date

2022-12-05

DOI

10.1085/jgp.202213193

Peer reviewed

JGP Journal of General Physiology

ARTICLE

The funny current I_f is essential for the fight-or-flight response in cardiac pacemaker cells

Colin H. Peters[1*], Christian Rickert[1*], Stefano Morotti[2], Eleonora Grandi[2], Kurt A. Aronow[3], Kurt G. Beam[1], and Catherine Proenza[1,4]

The sympathetic nervous system fight-or-flight response is characterized by a rapid increase in heart rate, which is mediated by an increase in the spontaneous action potential (AP) firing rate of pacemaker cells in the sinoatrial node. Sympathetic neurons stimulate sinoatrial myocytes (SAMs) by activating β adrenergic receptors (βARs) and increasing cAMP. The funny current (I_f) is among the cAMP-sensitive currents in SAMs. I_f is critical for pacemaker activity, however, its role in the fight-or-flight response remains controversial. In this study, we used AP waveform analysis, machine learning, and dynamic clamp experiments in acutely isolated SAMs from mice to quantitatively define the AP waveform changes and role of I_f in the fight-or-flight increase in AP firing rate. We found that while βAR stimulation significantly altered nearly all AP waveform parameters, the increase in firing rate was only correlated with changes in a subset of parameters (diastolic duration, late AP duration, and diastolic depolarization rate). Dynamic clamp injection of the βAR-sensitive component of I_f showed that it accounts for ∼41% of the fight-or-flight increase in AP firing rate and 60% of the decrease in the interval between APs. Thus, I_f is an essential contributor to the fight-or-flight increase in heart rate.

Introduction

The sympathetic nervous system fight-or-flight response is characterized by a rapid increase in heart rate that is mediated by pacemaker cells in the sinoatrial node. Sinoatrial node myocytes (SAMs) trigger each beat of the heart by firing spontaneous action potentials (APs) that propagate through the cardiac conduction system to initiate contraction (Keith and Flack, 1907). The sympathetic nervous system increases heart rate by accelerating this spontaneous AP firing rate. Within SAMs, the faster AP firing rate is caused by an increase in cytosolic cAMP following sympathetic activation of β adrenergic receptors (βARs) on the cell membrane. While a host of processes in SAMs are regulated directly and indirectly by the βAR-mediated increase in cAMP, the relative contributions of these processes to the fight-or-flight increase in AP firing rate remain unresolved.

APs in sinoatrial myocytes have a characteristic shape, which is determined by the unique complement of ion channels and transporters on the cell membrane. The changes to the sinoatrial AP waveform that occur with βAR stimulation could, in theory, serve as "fingerprints" to identify the ionic currents that mediate the increase in AP firing rate. However, the changes to the sinoatrial AP that occur with βAR stimulation have yet to be systematically defined, owing in part to (1) differences in experimental conditions and a lack of standard AP waveform definitions, which restrict comparisons between studies; (2) a focus on the diastolic depolarization rate (DDR) as the primary determinant of firing rate to the exclusion of other AP waveform parameters; and (3) the limited resolution of most studies owing to the heterogeneity of sinoatrial APs and difficulty of recording from large numbers of isolated SAMs.

The role of the hyperpolarization-activated funny current, I_f, in the fight-or-flight increase in AP firing rate in SAMs is the subject of longstanding debate (Lakatta and DiFrancesco, 2009; Bucchi et al., 2012; Hennis et al., 2021). I_f is a hallmark of SAMs and is critical for the generation of spontaneous APs (Bucchi et al., 2007; DiFrancesco, 2010; Baruscotti et al., 2011). I_f is produced by hyperpolarization-activated cyclic nucleotide-sensitive (HCN) channels, particularly HCN4, which is the predominant isoform in the sinoatrial node (Moosmang et al., 1999). Reduction in I_f through pharmacological blockers or mutations in HCN4 slows AP firing rate in SAMs and heart rate

[1]Department of Physiology & Biophysics, University of Colorado Anschutz Medical Campus, Aurora, CO; [2]Department of Pharmacology, University of California, Davis, School of Medicine, Davis, CA; [3]Redgarden Engineering, Boulder, CO; [4]Division of Cardiology, Department of Medicine, University of Colorado Anschutz Medical Campus, Aurora, CO.

*C.H. Peters and C. Rickert contributed equally to this paper. Correspondence to Catherine Proenza: catherine.proenza@cuanschutz.edu

This work is part of a special issue on Structure and Function of Ion Channels in Native Cells and Macromolecular Complexes.

in human patients and animal models (Bucchi et al., 2007; Swedberg et al., 2010; Baruscotti et al., 2011; Milano et al., 2014). Although βAR stimulation potentiates I_f, consistent with a role in increasing AP firing rate in SAMs (Brown et al., 1979), it has been argued that the contribution of I_f is negligible, owing in part to its low fractional activation at physiological potentials in SAMs and a residual βAR response in animal models with reduced expression or mutation of HCN4 (Lakatta and DiFrancesco, 2009; Alig et al., 2009; Mesirca et al., 2014; Hennis et al., 2021).

Although I_f is activated by membrane hyperpolarization, we recently showed that I_f is persistently active throughout the entire AP cycle in SAMs, owing to its very slow rates of activation and deactivation (Peters et al., 2021). The persistent activation of I_f allows it to conduct >50% of the net inward charge movement during diastole, despite its low fractional activation (Peters et al., 2021). Importantly, we also showed that the fraction of the net inward charge movement conducted by I_f increases to 93% of the total during βAR stimulation (Peters et al., 2021). The latter result strongly suggests that I_f contributes substantially to the fight-or-flight increase in heart rate.

In this study, we sought to quantitatively evaluate the role of I_f in the fight-or-flight increase in AP firing rate in SAMs. We began by analyzing a large data set of sinoatrial APs with automated AP waveform analysis, correlation analysis, and machine learning to identify the subset of AP waveform parameters that account for the majority of the βAR-mediated increase in AP firing rate. We then used dynamic clamp experiments to demonstrate that βAR-stimulation of I_f alone accounts for ∼41% of the chronotropic response to βAR stimulation in SAMs, mainly through effects during diastole. These results clearly establish that I_f contributes to the fight-or-flight increase in heart rate as part of a multifaceted cardiac pacemaking mechanism.

Materials and methods

Animal care and euthanasia

This study was carried out in accordance with the US Animal Welfare Act and the National Research Council's Guide for the Care and Use of Laboratory Animals and was conducted according to a protocol that was approved by the University of Colorado-Anschutz Medical Campus Institutional Animal Care and Use Committee. 6–8-wk old male C57BL/6J mice were obtained from Jackson Laboratories. Animals were anesthetized by isofluorane inhalation and euthanized under anesthesia by cervical dislocation and bilateral thoracotomy.

Acute isolation of murine sinoatrial myocytes

Sinoatrial myocytes were isolated as we have previously described (Sharpe et al., 2016; Larson et al., 2013). The heart was excised and the sinoatrial node dissected in Tyrode's solution (in mM: 140 NaCl, 5.4 KCl, 5.6 glucose, 5 HEPES, 1.8 $CaCl_2$, 1.2 KH_2PO_4, and 1 $MgCl_2$; pH adjusted to 7.4 with NaOH) containing 10 USP U/ml heparin (Sagent Pharmaceuticals) at 36°C. Strips of sinoatrial node tissue were subsequently rinsed in a low Ca^{2+} modified Tyrode's solution (in mM: 140 NaCl, 50 taurine, 5.4 mM KCl, 18.5 glucose, 5 HEPES, 1.2 KH_2PO_4, 0.066 $CaCl_2$, and 1 mg/ml BSA; pH adjusted to 6.9 with NaOH) at 36°C. The tissue was then digested for 25–30 min at 36°C in either 2 ml of the low Ca^{2+} Tyrode's containing 1.79 units protease type XIV (Sigma-Aldrich) and 0.54 units collagenase B (Sigma-Aldrich) or 5 ml of the low Ca^{2+} Tyrode's containing 1,064 units type II collagenase (Worthington), 9 units elastase (Worthington), and 652 µg type XIV protease (Sigma-Aldrich). After enzymatic digestion, the tissue was extensively rinsed in a modified Kraft-Brühe (KB) solution (in mM: 100 *K*-glutamate, 25 KCl, 20 glucose, 20 taurine, 10 *K*-aspartate, 10 KH_2PO_4, 5 creatine, 5 HEPES, 2 $MgSO_4$, 0.5 EGTA, and 1 mg/ml BSA; pH adjusted to 7.2 with KOH) at 36°C to prevent further enzymatic digestion. Individual sinoatrial myocytes were obtained by mechanical trituration of the digested tissue with a fire-polished glass pipette for 2–5 min in 2.5 ml of the KB solution. The calcium concentration of the cell suspension was gradually increased to a final concentration of 1.8 mM during a total adaptation time of 30 min. Cells were stored at room temperature for up to 6 h before recordings.

Electrophysiology

Aliquots of cells (∼100 µl) were transferred to a recording chamber on the stage of an inverted microscope, and cells were continuously perfused at 1–2 ml/min with Tyrode's solution with or without the βAR agonist, isoproterenol (Iso; 1 nM–10 µM). Bath and perfusing solutions were maintained at 35° ± 2°C with a feedback-controlled dual-channel temperature controller (TC-344B; Warner Instruments).

Spontaneously beating sinoatrial myocytes were patch-clamped in the Amphotericin B perforated patch configuration as previously described (Sharpe et al., 2017). Recording pipettes were pulled from borosilicate glass using a Sutter Instruments P-97 horizontal puller. Pipette resistances ranged from 1.5 to 3.3 MΩ with an average of 2.6 MΩ.

The patch pipette base solution contained (in mM) 135 KCl, 0.1 $CaCl_2$, 1 $MgCl_2$, 5 NaCl, 10 EGTA, 4 MgATP, and 10 HEPES; adjusted to pH 7.2 with KOH. A perforation stock solution was prepared by solubilizing 50 mg/ml Pluronic F-127 in DMSO (both from Sigma-Aldrich) and adding 20 mg/ml Amphotericin-B (Apexbio Technology LLC). 5–15 µl of the perforation stock solution was added to 500 µl of the pipette solution and solubilized by sonication for a final Amphotericin-B concentration of 0.2–0.6 mg/ml. This final perforation solution was prepared fresh each hour and kept on ice. Pipettes were tip-filled with the perforation solution by immersing them for ∼20 s. The pipette shafts were then back-filled with the amphotericin-free pipette base solution.

Cells were patch-clamped using an Axopatch 200B amplifier, Digidata 1440a A/D converter, and ClampEx software (Molecular Devices). Data were acquired at 50 kHz and low-pass filtered at 10 kHz. After establishing a high-resistance seal (>1 GΩ), the perforation progress was confirmed by a reduction in access resistance in voltage-clamp mode and by a visible minimization of maximum diastolic potential (MDP) to a stable value in fast current-clamp mode. After roughly 30 s of perforation time, the MDP regularly stabilized around −69 mV (Table S1), while the average membrane and access resistances were 457 ± 53 and 12.6 ± 0.6 MΩ (n = 61), respectively.

Spontaneous APs were recorded in the "I-Clamp Fast" current clamp mode using the initial extracellular perfusing solution until both MDP and FR were stable for at least 1 min, which usually occurred within 1–3 min after establishing a high-resistance seal. The perfusing solution was then changed to a different Iso concentration (e.g., from 1 nM Iso to 1 µM Iso). In general, firing rate stabilized at new levels within 30 s after the solution change and the recording was then continued for at least another 1 min to document the Iso-sensitive changes of AP waveform parameters. APs were recorded without compensation for series resistance because the voltage-offset is zero during recordings of spontaneous APs without an injected current and is negligible (<1 mV) with the small currents injected in the dynamic clamp experiments (see below).

We verified by two methods that the I-Clamp fast current-clamp circuit in the Molecular Devices Axopatch 200B amplifier faithfully reports sinoatrial AP waveforms. First, average sinoatrial APs recorded in 1 nM or 1 µM Iso were uploaded to a DG822 waveform generator (Rigol Technologies). These AP waveforms were input to the headstage of the Axopatch 200B amplifier through a circuit mimicking the access resistance (10 MΩ) and stray capacitance of (4.7 pF) the recording pipette and the signal was then recorded in I-Clamp fast mode (Fig. S1 A). As shown in Fig. S1, B and C, the recorded signals closely matched the input signals. Indeed, comparison of the input and measured signals using ParamAP software showed that the amplifier introduced negligible errors in sinoatrial AP waveform parameters (Table S4).

As an independent approach, we measured the response of the Axopatch 200B amplifier in the frequency range of the sinoatrial AP. The frequency content of sinoatrial APs was determined by fast Fourier transform analysis. As illustrated in Fig. S1 D, 99% of the information content of sinoatrial APs lies below 100 Hz. The frequency response of the amplifier in fast current clamp mode was then evaluated using a series of 100 mV peak-to-peak sine waves ranging in frequency from 0.1 Hz to 20 kHz. As shown in Fig. S1, E and F, there were minimal distortions in amplitude or phase in the frequency range corresponding to the sinoatrial AP.

Dynamic clamp experiments

For dynamic clamp experiments, we modified an Arduino-based system (Desai et al, 2017) to better match the system's digital output range with the current command input range of the Axopatch 200B patch clamp amplifier. Control and feedback from the system were measured using the custom open-source "pyClamp" (Rickert and Proenza, 2019a) user client and "dyClamp" (Rickert and Proenza, 2019b) host controller software sketches.

Dynamic current-clamp recordings from SAMs were performed in the perforated-patch clamp configuration as described above. SAMs were continuously perfused with Tyrode's solution containing either 1 nM or 1 µM Iso and baseline APs were recorded without current injection until both FR and MDP were stable (~1 min). The membrane potential measured from the cells was used to calculate simulated I_f currents in a 10 µs feedback loop from previously described Hodgkin–Huxley models of I_f (Peters et al., 2021; Fig. S2 A). Two I_f models were used, one describing I_f in 1 nM Iso and the other describing I_f in 1 µM Iso. The models were originally parameterized to match I_f recorded from SAMs in response to families of hyperpolarizing voltage steps; they were subsequently validated against I_f measured in AP clamp experiments across a range of AP firing rates (200–400 bpm in 1 nM Iso, and 250–470 bpm in 1 µM Iso; Peters et al., 2021).

In the dynamic clamp experiments in the present study, both models of I_f were simulated in response to the recorded membrane voltage and the Iso-sensitive component of I_f ($I_{f\text{-}Iso}$) was calculated as the difference between the simulated 1 nM and 1 µM currents ($I_{f,\mu M}$–$I_{f,nM}$) at each time step. $I_{f\text{-}Iso}$ was then added as an injected current-clamp current to cells perfused with 1 nM Iso to simulate the effects on the AP waveform and firing rate of βAR stimulation of I_f. Similarly, $I_{f\text{-}Iso}$ was subtracted from cells perfused with 1 µM Iso to simulate the effects of removing βAR stimulation of I_f. This approach is illustrated schematically in Fig. S2 B.

In initial experiments (shown in Fig. 4), $I_{f\text{-}Iso}$ was injected in a series of steps of increasing maximum conductance from 5 to 40 nS, which corresponded to current injections of approximately 1–25 pA. The open-probability and driving force of the models were updated from the measured voltage at each time step to obtain the "instantaneous" I_f conductance and current; however, because open probability changes little over the course of the AP (Peters et al., 2021), time-dependent changes in the injected current at different potentials primarily reflect changes in driving force. Dynamic current injections were monitored with both the current command input to the amplifier and the 10-kHz-filtered head stage signal returned from the amplifier. For each conductance level, currents were injected for ~1 min to allow both MDP and/or FR to stabilize. The stable APs recorded during the latter part of the current injection time were then analyzed.

To measure the cell-specific effects of βAR stimulation of I_f (Figs. 5 and 6), $I_{f\text{-}Iso}$ was injected into SAMs with the maximal conductance incremented in steps of 2 nS for 15 s each up to 20 nS. Then the dynamic clamp was turned off and 1 µM Iso was perfused in the absence of injected current to determine the full cell-specific βAR response (Fig. 5 A). The amplifier was switched to voltage-clamp mode and whole-cell access was gained to measure cellular capacitance. On average in this configuration, the membrane resistance was 405 ± 98.0 MΩ, the access resistance was 4.6 ± 0.4 MΩ, and the cellular capacitance was 35.0 ± 3.7 pF (n = 10–13). Cells were then perfused with Tyrode's containing 1 mM $BaCl_2$ (to block inward rectifier K^+ currents, the only other active conductance at hyperpolarized potentials; DiFrancesco et al., 1986; Giles and Imaizumi, 1988) and I_f was measured as the time-dependent current elicited by a 3 s voltage step to −130 mV, at which potential the channels are fully activated (Peters et al., 2021; Fig. 5 B). The cell-specific maximal I_f conductance (G_f) was calculated offline using Eq. 1:

$$G_f = \frac{I_{f,-130}}{V_m - E_{rev}} * Po^{-1}, \quad (1)$$

where $I_{f,-130}$ is the amplitude of the time-dependent inward current at −130 mV, V_m is the membrane potential (−130 mV), E_{rev} is the reversal potential of I_f (−30 mV), and P_o is the predicted steady-state open probability of the 1 µM Iso model at −130 mV (~100%). The FR and AP waveform during the dynamic injection with the conductance closest to that measured in the cell were then compared to those measured in the same cell in 1 µM Iso to determine the fractional contribution of I_f to the total βAR response in each cell (Fig. 5 C and Fig. 6). Because the firing rate runs-down slightly during the protocol (typically <20 AP/min over 10 min), the temporally closest 1 nM recording was used for comparison to each of dynamic injection and βAR stimulation (Fig. 6 B).

Action potential waveform analysis with ParamAP

AP waveforms were parameterized using ParamAP software (Rickert and Proenza, 2017; Rickert and Proenza, 2021). Segments of stable APs were extracted from the recordings and saved in Axon's text file (ATF) format before being analyzed with ParamAP. Variable length analysis windows were used to capture APs with stable features and membrane parameters and to avoid noise artifacts. In addition to previously described parameters, ParamAP was updated to include the late-action potential duration (LAPD), which measures the time in diastole preceding the maximum diastolic potential. All parameter definitions are listed in Table 1. As a validation for sufficient parameterization, the measured waveform parameters captured by ParamAP from individual cells can be used to recapitulate sinoatrial APs with linear segments defined by said parameters (Fig. S3 B).

Machine learning

We used machine learning to predict the changes in SAM firing rate given measured changes in AP waveform parameters (Table 1). We constructed 100 random forest models, each populated with 1,000 trees, using the scikit-learn Python module (Pedregosa et al., 2011). Models between 50 and 5,000 trees were tested, and similar results obtained for each model, with 1,000 and 5,000 tree models showing less variability between any given forest. Each of the random forests was generated with a pseudo-random starting point to generate a range of feature importance measures. Models were trained on the dataset of 50 cells recorded in 1 nM and 1 µM Iso to predict the fractional change in firing rate with βAR stimulation. The predicting variables were chosen to measure all relevant periods, membrane potentials, and rates, while excluding redundant variables reporting on subsets of the AP waveform already included within another predictor. For example, APD_{50} was not included as that region of the AP-waveform is a subset of the data included in the APD_{90} variable. Models were tested against the effects of βAR stimulation in the independent dataset of cells used for dynamic clamp analysis and were capable of predicting the change in firing rate with an average error of 12.2% (approximately the standard error of the mean for the firing rate change in the training and targets datasets, which were 13.4 and 11.0%, respectively). Predictor importance was measured by evaluating the contribution of each parameter to reducing node impurity within the training data set using the default function within the scikit-learn module. Thus, importance is both a measure of the frequency with which a predictor appears within the forest and its ability to split data into less variable subgroups.

Statistical analysis

All statistical analysis was performed in JMP 15 (SAS Institute). Comparisons of unmatched 0 nM, 1 nM, 1 µM, and 10 µM Iso were performed using a one-way ANOVA. Pairwise comparisons were performed using a Tukey post-hoc test. Comparisons of matched 1 nM and 1 µM Iso datasets were performed using paired *t* tests. Comparisons in dynamic clamp experiments were performed using paired *t* tests with a Bonferroni correction of 2 used for multiple pairwise comparisons (1 nM Iso versus dynamic and 1 µM-1 nM Iso versus dynamic-1 nM Iso). Correlations between parameters were calculated using a Pearson correlation coefficient. Statistical significance was set at $P < 0.05$.

Online supplemental material

Fig. S1 shows Axon Axopatch 200B validation. Fig. S2 shows dynamic clamp approach. Fig. S3 shows ParamAP automates determination of sinoatrial node AP waveform parameters and fully parameterizes the AP. Table S1 shows Pearson correlation coefficients between firing rate and waveform parameters in 1 nM and 1 µM Iso. Table S2 shows dynamic clamp changes in AP firing rate and AP waveform. Table S3 shows DDR in cells binned by firing rate. Table S4 shows errors in sinoatrial AP waveform parameters introduced by the Axopatch 200B amplifier.

Results

Most sinoatrial AP waveform parameters change in response to βAR stimulation

To define the effects of βAR stimulation on the sinoatrial AP waveform, we recorded spontaneous APs in the amphotericin perforated-patch configuration in 50 sinoatrial myocytes from 24 mice. In each cell, APs were first recorded in a control extracellular solution containing 1 nM of the βAR agonist Iso and then upon wash-on of 1 µM Iso. 1 nM Iso was used in the control solution as in previous studies (Larson et al., 2013; Peters et al., 2021) because it mimics the resting catecholamine levels in mice (Pichavaram et al., 2018; Lucot et al., 2005) and humans (Messan et al., 2017). We confirmed that 1 nM Iso did not increase AP firing rate compared to a solution lacking Iso (304 ± 15 bpm in 1 nM, $n = 50$ vs. 313 ± 31 bpm in 0 nM, $n = 19$; $P = 0.9879$). 1 µM Iso was used as the stimulated condition as previously (Larson et al., 2013; Fenske et al., 2020; Peters et al., 2021) and we confirmed 1 µM Iso to be a saturating concentration, as 10 µM Iso did not produce a further increase in AP firing rate (400 ± 12 bpm in 1 µM, $n = 50$ vs. 400 ± 33 bpm in 10 µM, $n = 9$; $P = 1.0000$).

AP firing rate and AP waveform parameters in the control and Iso-stimulated conditions were determined by automated analysis with ParamAP software (Rickert and Proenza, 2017; Rickert and Proenza, 2021). ParamAP defines 15 AP waveform parameters, including time intervals, membrane potentials, and rates of change of membrane potential, which together provide a

Table 1. **AP waveform parameter definitions**

Waveform parameter	Abbreviation	Definition
Firing rate	FR (AP/min)	Number of APs fired per minute
Diastolic duration	DD (ms)[a]	Time from maximum diastolic potential until the threshold potential
Early diastolic duration	EDD (ms)	Time from maximum diastolic potential until the rate of depolarization deviates from a linear fit
Late diastolic duration	LDD (ms)	Time from when the rate of diastolic depolarization deviates from a linear fit until threshold
Action potential duration	APD (ms)	Time interval between the threshold potential during AP upstroke and the subsequent maximum diastolic potential
Action potential duration at 50% repolarization	APD_{50} (ms)	Time interval for 50% repolarization
Action potential duration at 90% repolarization	APD_{90} (ms)[a]	Time interval for 90% repolarization
Late action potential duration	LAPD (ms)[a]	Time from when the threshold potential is reached during the repolarization phase until the subsequent maximum diastolic potential
Maximum diastolic potential	MDP (mV)[a]	Most negative membrane potential during diastolic depolarization phase
Threshold	THR (mV)[a]	Time at which the upstroke velocity reaches 0.5 mV/ms
Peak potential	PP (mV)[a]	Most positive potential during the AP upstroke
Action potential amplitude	APA (mV)	Difference between maximum diastolic potential and peak potential
Diastolic depolarization rate	DDR (mV/ms)[a]	Rate of the membrane potential change at the end of the early diastolic duration
Maximum upstroke velocity	MUV (mV/ms)[a]	Maximum of the derivative between maximum diastolic potential and peak potential
Maximum repolarization rate	MRR (mV/ms)[a]	Minimum of the derivative between peak potential and the subsequent maximum diastolic potential

[a]Denotes AP waveform parameters used in the machine learning predictions of firing rate.

full description of sinoatrial APs (Table 1 and Fig. S3). Although AP waveforms recorded in individual cells exhibited considerable heterogeneity (Fig. 1, A and B), characteristic features of sinoatrial APs were apparent in the recordings, including a spontaneous diastolic depolarization, depolarized MDP, slow maximum upstroke velocity (MUV), and small AP amplitude (APA; Table 2).

We performed correlation analysis to identify the AP waveform parameters that are significantly associated with AP firing rate (Fig. 1, C–E; and Table S1). We found that firing rate was significantly correlated with the duration of both early and late phases of the diastolic depolarization (EDD and LDD), with all measures of AP duration (APD), and with the DDR in both 1 nM and 1 µM Iso, while the maximum repolarization rate (MRR) was correlated with firing rate only in 1 µM Iso. Interestingly, firing rate was not significantly correlated with MDP or any other parameter reporting membrane voltage or with the upstroke velocity.

We next examined the changes in the AP waveform that occur in response to βAR stimulation. As expected, the AP firing rate was significantly greater in 1 µM Iso than in 1 nM Iso (Table 2 and Fig. 2 B). This increase in firing rate was accompanied by significant changes in every AP waveform parameter except APD_{50} (Table 2 and Fig. 2, B–E). βAR stimulation shortened time intervals in the AP including the EDD, LDD, APD_{90}, and LAPD. It also changed membrane potentials by hyperpolarizing the MDP and threshold (THR), depolarizing the peak potential (PP) and increasing the APA. Finally, βAR stimulation sped rates of change of membrane potential, increasing the DDR, MUV, and MRR.

Overall, these data are consistent with a coordinated response of many Iso-sensitive currents during βAR stimulation. However, they do not provide information about the relative importance of different AP parameters in determining the increase in firing rate with βAR stimulation.

DDR and LAPD are the primary predictors of the βAR increase in firing rate

We used two independent approaches to identify the AP waveform parameters that are the most important determinants of the Iso-dependent increase in AP firing rate. First, we calculated Pearson correlation coefficients to assess how Iso-induced changes in each AP waveform parameter relate to the increase in firing rate (Table S1 and Fig. 3, A–C). Unsurprisingly, the increase in firing rate in response to 1 µM Iso was significantly correlated with decreases in the time intervals that make up the total cycle length, including the diastolic duration (DD) and the total APD. Within the diastolic duration, decreases in both EDD and LDD were significantly associated with the increase in firing rate (Fig. 3, A1 and A2). However, of the parameters comprising the total APD, only a decrease in LAPD was significantly correlated with increased firing rate (Fig. 3, C1–C3). The DDR was the only non-interval parameter that was significantly correlated with the increase in firing rate (Fig. 3 A4).

We next used a machine-learning approach as an independent means to identify the waveform parameters that are the most important predictors of the βAR-stimulated increase in firing rate. We used 100 random forests, each containing 1,000 decision trees (Breiman, 2001), to evaluate the importance of a subset of non-redundant AP waveform parameters (marked by asterisks in Table 1). Consistent with the results of the correlation analysis, machine-learning identified changes to DD, LAPD, and DDR as significantly associated with the βAR-induced increase in AP firing rate (Fig. 3 D). Taken together, these results

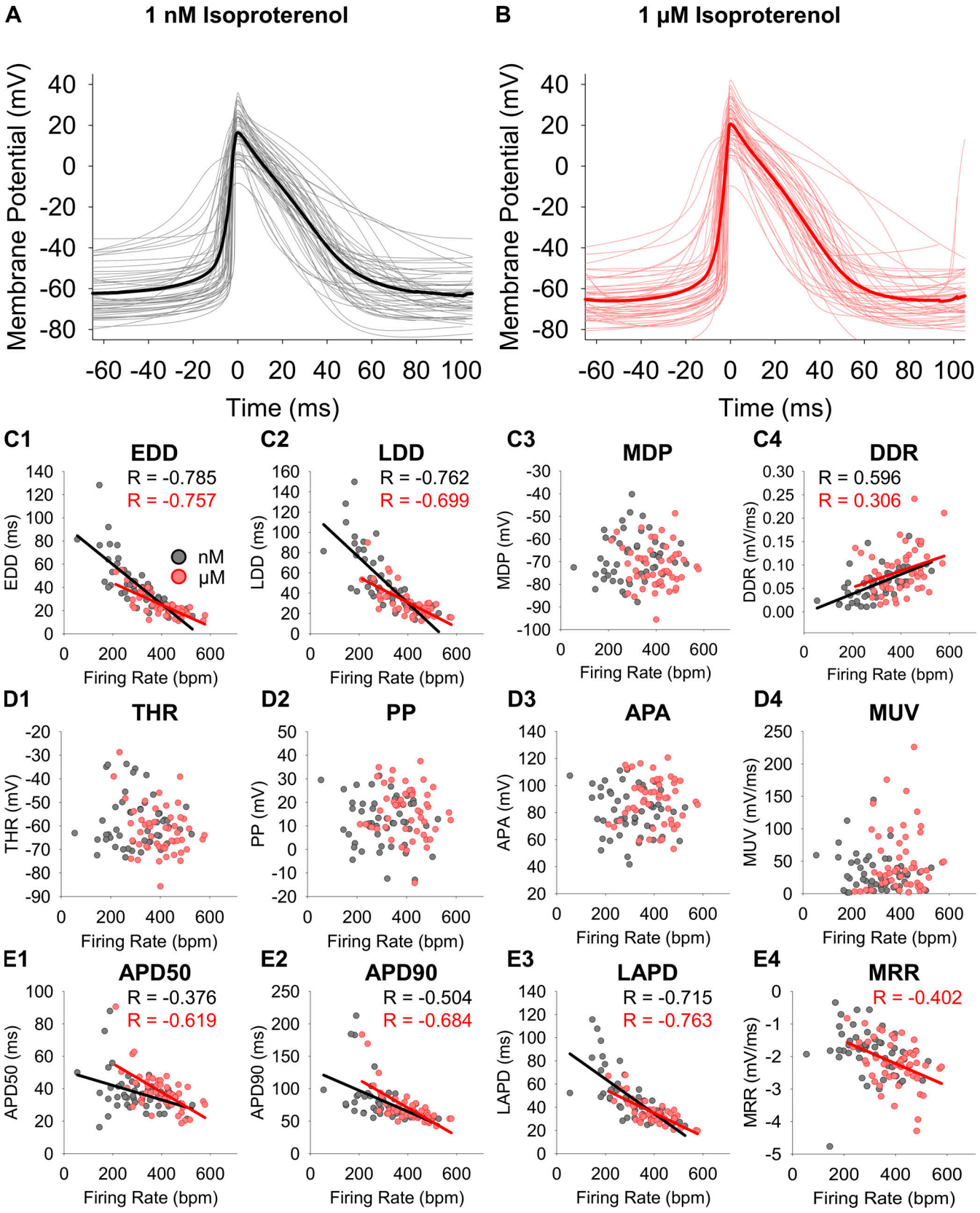

Figure 1. **Sinoatrial action potentials are heterogeneous. (A)** Overlays of individual (n = 50) sinoatrial AP waveforms (grey) and the average of all waveforms (black) recorded in 1 nM Iso. **(B)** Overlays of individual (n = 50) sinoatrial AP waveforms (pink) and the average of all waveforms (red) recorded in 1 µM Iso. **(C–E)** Correlation plots of individual AP waveform parameters in 1 nM Iso (grey) and 1 µM Iso (pink) as a function of the AP firing rate. Significant correlations are shown as black (1 nM) and red (1 µM) lines, and the Pearson correlation coefficients are noted. All correlation coefficients and details of statistical tests can be found in Table 2.

Table 2. **Average (±SEM) AP firing rate and waveform parameters in 1 nM and 1 µM Iso**

	1 nM Iso	1 µM Iso	P value 1 nM vs. 1 µM
FR (bpm)	304 ± 14	400 ± 12	P < 0.0001[a]
DD (ms)	93.7 ± 7.1	55.9 ± 3.5	P < 0.0001[a]
EDD (ms)	41.9 ± 3.1	25.0 ± 1.5	P < 0.0001[a]
LDD (ms)	51.7 ± 4.3	30.9 ± 2.1	P < 0.0001[a]
MDP (mV)	−68.7 ± 1.4	−72.0 ± 1.3	P = 0.0013[a]
DDR (mV/ms)	0.060 ± 0.005	0.087 ± 0.007	P < 0.0001[a]
THR (mV)	−58.3 ± 1.5	−61.9 ± 1.5	P = 0.0007[a]
PP (mV)	11.9 ± 1.5	16.2 ± 1.5	P < 0.0001[a]
APA (mV)	81.0 ± 2.5	88.3 ± 2.4	P < 0.0001[a]
MUV (mV/ms)	32.6 ± 4.1	51.0 ± 7.0	P = 0.0007[a]
APD (ms)	116.8 ± 5.1	99.6 ± 3.3	P < 0.0001[a]
APD_{50} (ms)	37.4 ± 1.7	37.9 ± 1.7	P = 0.5651
APD_{90} (ms)	80.3 ± 4.7	70.5 ± 3.7	P = 0.0003[a]
LAPD (ms)	48.8 ± 3.0	34.9 ± 1.6	P < 0.0001[a]
MRR (mV/ms)	−1.9 ± 0.1	−2.2 ± 0.1	P < 0.0001[a]

n = 50 for all cases.
[a]Significant correlation (P < 0.05).

indicate that the interval between APs, including the LAPD, is the most important predictor of the increase in AP firing rate. It follows that the ionic currents that are active at sub-threshold membrane potentials are the primary drivers of the βAR-driven increase in sinoatrial node firing rate.

Iso stimulation of I_f accounts for 41% of the βAR firing rate increase

Although many Iso-sensitive currents are active at subthreshold potentials, our previous study showed that Iso stimulation increases I_f from ∼50 to >90% of the net inward current during each AP (Peters et al., 2021). Therefore, we sought to determine the degree to which this increase in I_f accounts for the increase in AP firing rate in SAMs, independent of the contribution of other Iso-sensitive currents. To this end, we employed the dynamic clamp approach using custom dynamic clamp hardware (Desai et al, 2017) and software (Rickert and Proenza, 2019a; Rickert and Proenza, 2019b). As shown schematically in Fig. S2 A dynamic clamp is a hybrid experimental-computational method, in the membrane voltage measured from a patch-clamped cell is used to calculate simulated currents from mathematical models which are then injected back into the same cell in a fast (10 µs) feedback loop.

In these experiments, we used our previously published Hodgkin-Huxley type models of I_f in 1 µM and 1 nM Iso (Peters et al., 2021). In current-clamp experiments, $I_{f\text{-}Iso}$ was dynamically calculated from voltages measured at ∼10 µs intervals from spontaneously firing SAMs patch-clamped in the amphotericin perforated patch configuration. The open probability and driving force in the 1 µM and 1 nM Iso models of I_f were updated from the measured voltage to obtain the predicted current. The Iso-sensitive component of I_f ($I_{f\text{-}Iso}$) was defined as the difference between the 1 µM and 1 nM models. $I_{f\text{-}Iso}$ was then either added to cells perfused with 1 nM Iso or subtracted from cells perfused with 1 µM Iso to determine the effects on the AP of βAR-stimulation of I_f. The resulting changes in the AP firing rate and AP waveform parameters were then compared to those recorded in the same cell before the current injection. The overall approach is illustrated schematically in Fig. S2.

As an initial proof of concept, spontaneously firing cells perfused with 1 nM Iso were dynamically injected with $I_{f\text{-}Iso}$ of increasing maximal conductance ranging from 5 to 40 nS (Fig. 4 A). We found that an average maximal I_f conductance of 10 nS was sufficient to significantly increase the AP firing rate and larger injections of I_f caused larger increases in firing rate (Fig. 4, C and D). In accordance, when the reverse experiment was performed and $I_{f\text{-}Iso}$ was subtracted from SAMs perfused with 1 µM Iso, a 10 nS maximal I_f conductance was sufficient to significantly reduce the AP firing rate (Fig. 4, B and D). Given our prior report showing an average maximum conductance of I_f of 11.79 ± 1.39 nS in SAMs (Peters et al., 2021), these results indicate that βAR stimulation of I_f contributes to the fight-or-flight increase in AP firing rate in SAMs.

In the next set of experiments, we scaled the conductance of the injected current to the endogenous I_f measured in each cell. In this dynamic clamp protocol, the conductance of the injected βAR-stimulated I_f was progressively increased in 2 nS steps (Fig. 5 A) and the appropriate conductance for each cell was determined post hoc by measuring the endogenous I_f during hyperpolarizing pulses following the dynamic clamp recordings (Fig. 5 B). The endogenous current was measured after the dynamic clamp recordings to allow the use of the inward-rectifier blocker Ba^{2+} in the isolation of I_f, as in many previous reports (Larson et al., 2013; DiFrancesco et al., 1986; Giles and Imaizumi, 1988; Liao et al., 2010; Sharpe et al., 2017). Finally, the firing rate and waveform parameters from the scaled dynamic clamp recording were compared to those of APs recorded in 1 nM and 1 µM Iso in the same cell in the absence of current injection (Fig. 5 C).

On average the cell-scaled peak $I_{f\text{-}Iso}$ inward current injected during the diastolic depolarization was −9.3 ± 1.1 pA (*n* = 13; Fig. 6 A, bottom), remarkably similar to the 9 pA difference measured between the peak inward I_f currents in AP clamp experiments in 1 nM and µM Iso (Peters et al., 2021). Injection of cell-scaled βAR-stimulated I_f significantly increased the firing rate by 59 ± 9 AP/min (+22.2% compared to 1 nM Iso; Table S2 and Fig. 6). This increase in firing rate due to βAR stimulation of I_f accounted for 41% of the increase in FR seen in response to perfusion of 1 µM Iso (143 ± 24 AP/min; +62.0% compared to 1 nM Iso; Table S2 and Fig. 6). These data conclusively establish that βAR stimulation of I_f contributes significantly to the fight-or-flight increase in AP firing rate in individual SAMs. Importantly, the data clearly indicate that I_f does not account for the full firing rate increase, which must include contributions from other currents.

We next analyzed the effects of dynamic injection of $I_{f\text{-}Iso}$ on the AP waveform parameters identified by correlation analysis and machine learning as the primary drivers of the

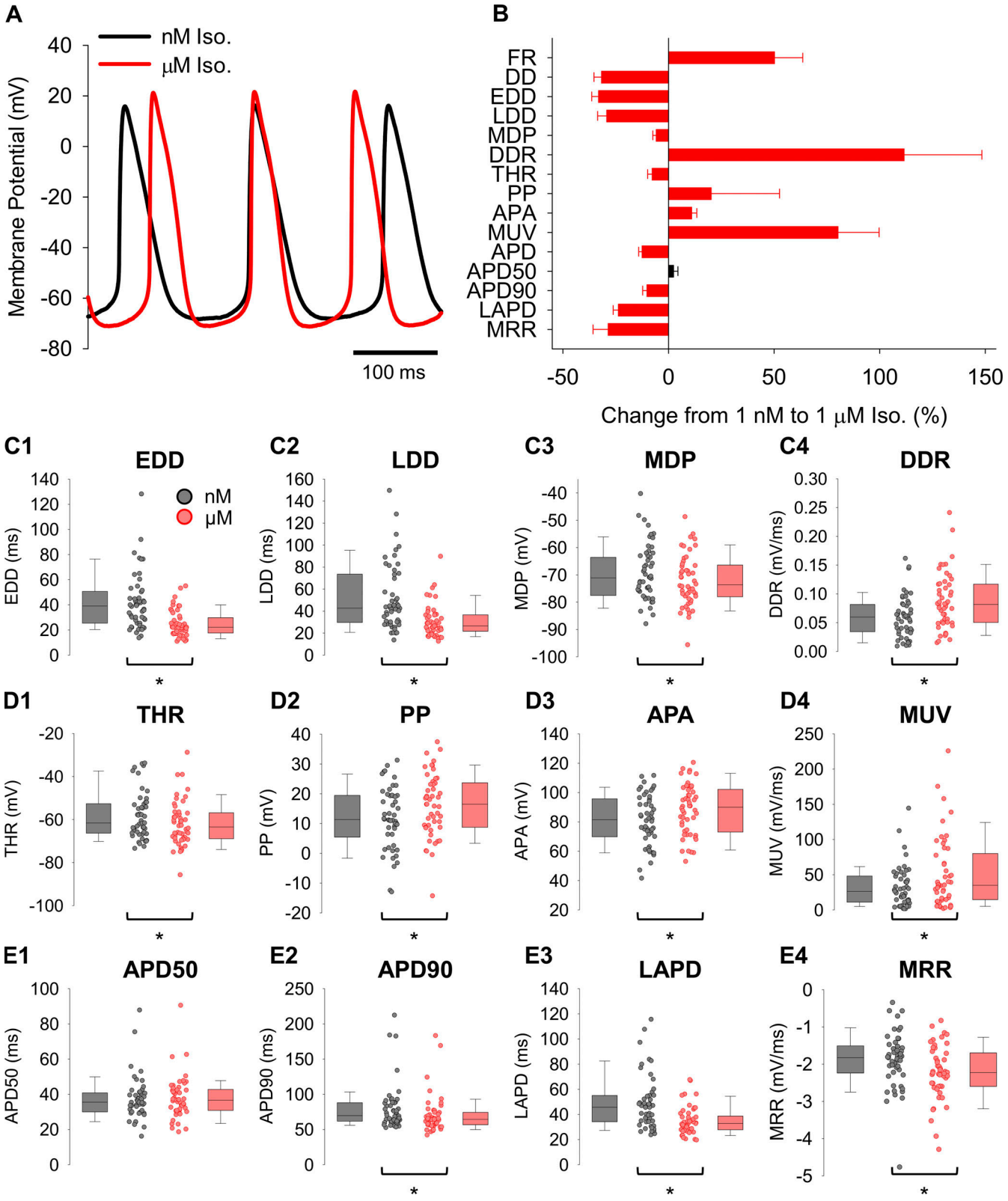

Figure 2. **Iso affects most sinoatrial AP waveform parameters. (A)** Representative sinoatrial APs recorded from a single cell in 1 nM Iso (black) and following wash-on of 1 μM Iso (red). **(B)** Average (±SEM) percentage change in sinoatrial AP firing rate and waveform parameters induced by perfusion of 1 μM Iso. Red bars denote parameters that are significantly different after βAR stimulation. Since MDP and MRR are negative numbers, a negative percentage change is equivalent to hyperpolarization of the MDP and an increase in the magnitude of MRR. **(C1–E4)** Box plots of median waveform parameters associated with the diastolic depolarization (C1–C4), action potential voltages and upstroke (D1–D4), and action potential duration and repolarization (E1–E4) in 1 nM Iso (grey) and 1 μM Iso (pink). Individual recordings in C–E are shown as circles. Asterisks indicate significant differences between 1 nM and 1 μM Iso. *n* = 50 for all cases. Details of statistical tests are found in Table 2.

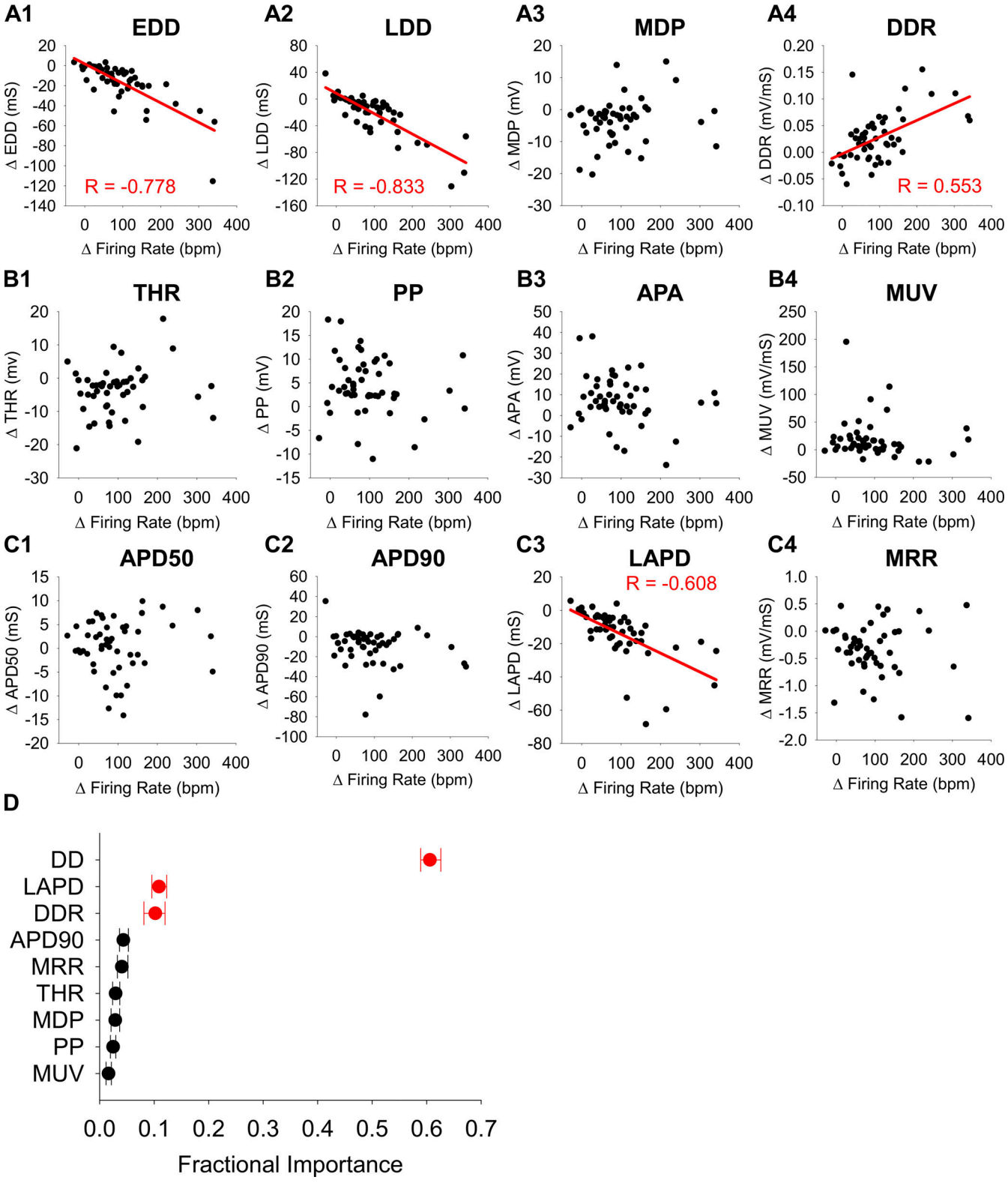

Figure 3. **βAR stimulation accelerates AP firing by shortening the diastolic interval. (A1–E4)** Correlation plots of the change in waveform parameters associated with diastolic depolarization (A1–A4), action potential upstroke (B1–B4), and action potential duration (C1–C4) versus the change in firing rate in SAMs between 1 nM and 1 µM Iso. Significant correlations are shown as a red line, and the Pearson correlation coefficient is noted. *n* = 50 for all cases. All correlation coefficients and details of statistical tests can be found in Table S1. **(D)** Average importance of changes to waveform parameters during βAR stimulation in predicting concomitant changes in AP firing rate as measured by random forest machine learning analysis. Variables that were significantly correlated with changes in firing rate in A–C are shown in red. Error bars show the minimum and maximum values obtained from the 100 forests modeled.

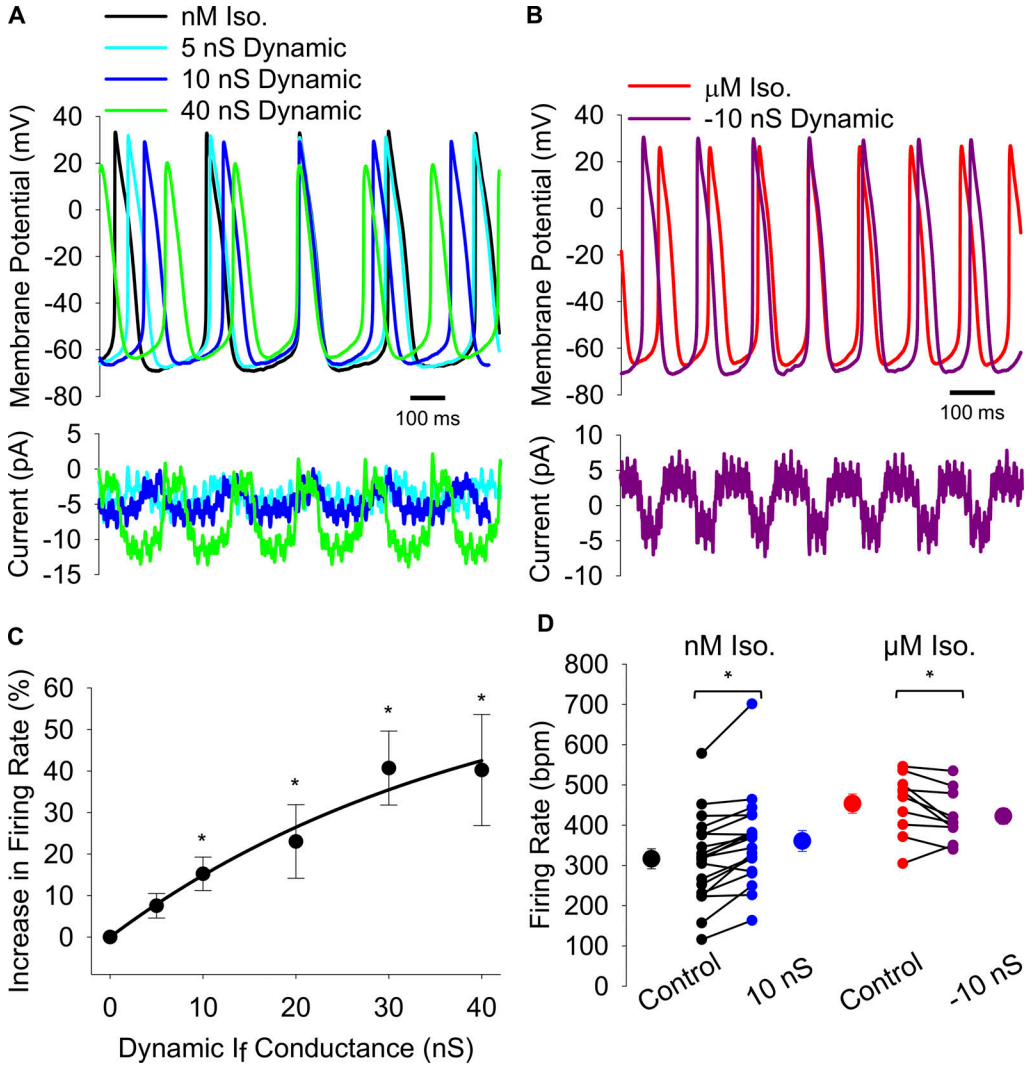

Figure 4. **Dynamic injection of βAR-stimulated I_f changes AP firing rate. (A)** Representative sinoatrial APs (top) recorded in 1 nM Iso with no current injection (black) and with dynamic addition of βAR stimulated I_f (bottom) with a conductance of 5 nS (teal), 10 nS (blue), or 40 nS (green). **(B)** Representative sinoatrial APs recorded in 1 µM Iso (top) without current injection (red) and with dynamic subtraction of βAR-stimulated I_f (bottom) with a conductance of 10 nS (purple). **(C)** Average (±SEM) fractional increase (%) in sinoatrial AP firing rate with dynamic injection of βAR-stimulated I_f at conductances between 5 and 40 nS. Injections of 10 nS or greater caused significant acceleration of the AP firing rate compared to control (5 nS—P = 0.9376, *n* = 19; 10 nS—P = 0.0401, *n* = 19; 20 nS—P = 0.0013, *n* = 17; 30 nS—P = 0.0003, *n* = 7; 40 nS—P < 0.0001, *n* = 14). **(D)** Average (±SEM) firing rate of cells perfused with 1 nM (black) or 1 µM Iso (red) before (Control) and after dynamic addition (blue) or subtraction (purple) of βAR-stimulated I_f (10 nS). Individual recordings are shown as smaller circles (*n* = 19 in 1 nM Iso and *n* = 10 in 1 µM Iso). Dynamic subtraction of βAR-stimulated I_f significantly reduced the AP firing rate compared to 1 µM Iso (P = 0.0402).

firing rate increase with βAR stimulation, namely, EDD, LDD, DDR, and LAPD. We found that $I_{f\text{-}Iso}$ accounted for 80% of the decrease in LAPD, 50% of the decrease in DD, and 40% of the decrease in LDD seen with perfusion of 1 µM Iso (Table S2 and Fig. 7, A and B). While dynamic injection of $I_{f\text{-}Iso}$ elicited trends toward faster DDR and shorter EDD, these effects were not statistically significant and the effects in individual cells were variable. Ultimately, these data suggest that βAR stimulation of I_f contributes to the fight-or-flight heart rate increase through shortening of the diastolic depolarization and late repolarization phases of the sinoatrial AP resulting in a 60% reduction in the time between APs.

Discussion

The sympathetic nervous system fight-or-flight increase in heart rate is among the most fundamental of physiological responses in mammals. Yet despite decades of research, the mechanisms underlying the increase in spontaneous AP firing rate in SAMs remain unresolved (Lakatta and DiFrancesco, 2009; Bucchi et al., 2012; Hennis et al., 2021). In this study, we first show that while virtually all aspects of the sinoatrial AP are changed by βAR stimulation, the magnitude of the fight-or-flight increase in firing rate is mediated by changes in only a subset of AP waveform parameters. Importantly, this subset of parameters constrains the list of βAR sensitive processes that primarily contribute to the fight-or-flight response in SAMs to those that are active at

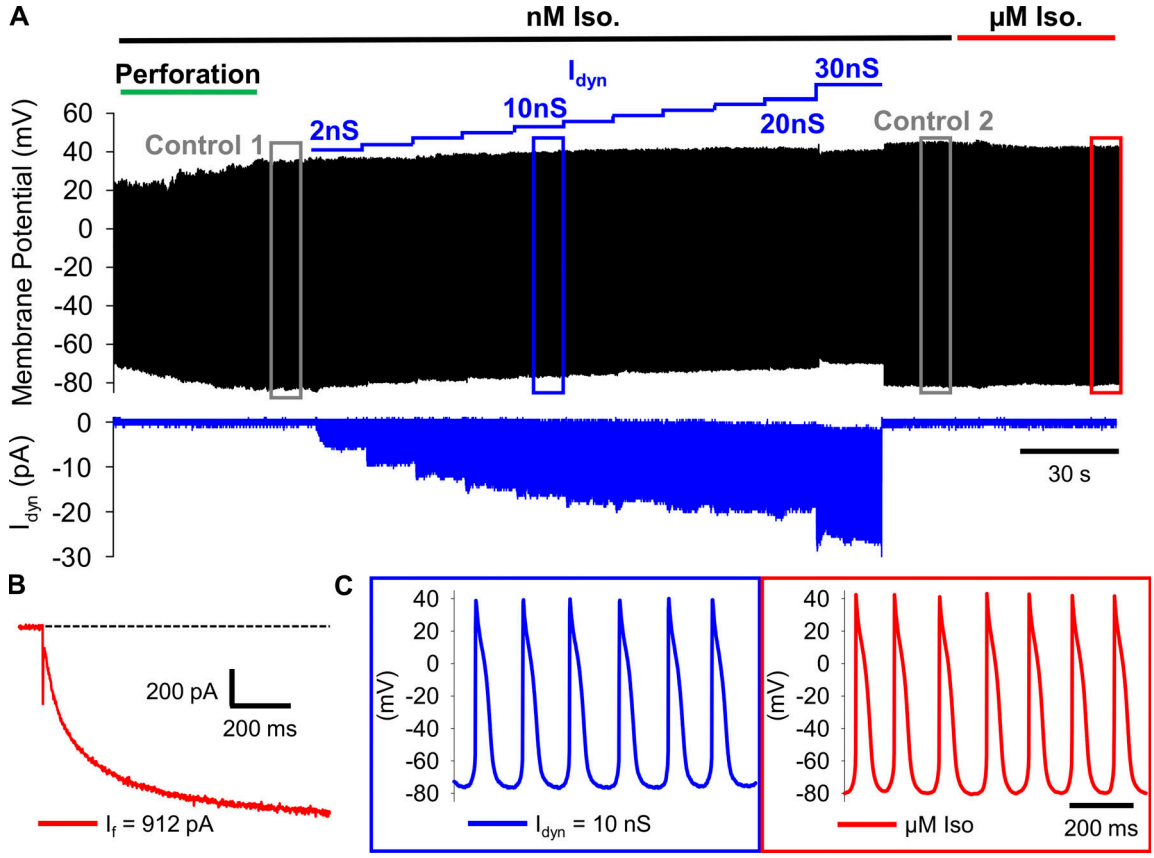

Figure 5. **Cell-scaled dynamic clamp approach. (A–C)** Protocol for dynamic clamp recordings with simulated conductance scaled to endogenous I_f. **(A)** Spontaneous APs are recorded from a cell perfused with 1 nM Iso (top) and dynamic clamp current is monitored (bottom). After AP amplitude stabilizes following perforation (green), the set of control APs are recorded (gray box), after which the dynamic clamp circuit is switched on and the maximal I_f conductance used to calculate the injected current (I_{dyn}) is increased in 2 nS steps (blue). Following the injected conductance series, the dynamic clamp circuit is switched off, a second set of control APs are recorded, and the cell is perfused with 1 μM Iso to measure the full βAR-stimulated response (red). **(B)** Following the control, dynamic current clamp, and Iso-stimulated recordings of APs in current-clamp mode, the amplifier is changed to voltage-clamp mode. 1 mM Ba^{2+} is perfused to block inward rectifier currents, and the endogenous I_f conductance is calculated from the current elicited by a voltage-step to −130 mV, where the current is >90% activated. In this example, conductance was calculated as 9.58 nS based on the 912-pA current and I_f reversal potential of −30 mV. **(C)** The endogenous I_f is then used to post hoc determine the dynamic clamp conductance for which the AP firing rate and waveform will be analyzed (blue).

subthreshold voltages. We then quantitatively establish that I_f accounts for about 41% of the increase in AP firing rate, countering previous claims that I_f does not play a role in this process.

βAR stimulation increases firing rate through a subset of AP waveform parameters

Numerous studies have suggested that βAR stimulation increases AP firing rate in SAMs at least in part by increasing the DDR (Zhang and Vassalle, 2003; Bucchi et al., 2007; Verkerk et al., 2012; Larson et al., 2013; Protze et al., 2017). However, more definitive determination of the sinoatrial AP waveform changes that mediate the fight-or-flight increase in firing rate have been hampered by inconsistent parameter definitions and small datasets. Our use of automated AP waveform analysis of a large dataset provides the necessary resolution to conclusively show that βAR stimulation significantly alters almost all AP waveform parameters—consistent with the host of βAR-sensitive processes in SAMs.

Importantly, however, our results (Fig. 3) also constrain the list of βAR-sensitive processes involved in the fight-or-flight response in SAMs by showing that a subset of sub-threshold parameters—namely EDD, LDD, DDR, and LAPD—are the key determinants of AP firing rate and the βAR-mediated increase in firing rate. This finding quantitatively confirms prior suggestions that shortening of the interval between APs and currents active during this phase are the main drivers of autonomic regulation of heart rate (Bucchi et al., 2007; DiFrancesco, 2010), although the beating rate of the intact sinoatrial node is also clearly influenced by other factors such as connectivity between sinoatrial cells (Boyett et al., 2000; Maltsev et al., 2022). In contrast, changes in systolic parameters such as shortening of the APD_{90} only account for 10–20% of the total change in cycle length and differ little between cells with small and large βAR-stimulated firing rate increases (Fig. 3 C2).

Evaluation the role of I_f in the fight-or-flight response is complicated by reduced resting rates

Whether and to what degree I_f is responsible for cardiac pacemaking and autonomic regulation of heart rate has long been debated (Lakatta and DiFrancesco, 2009; Hennis et al., 2021). On

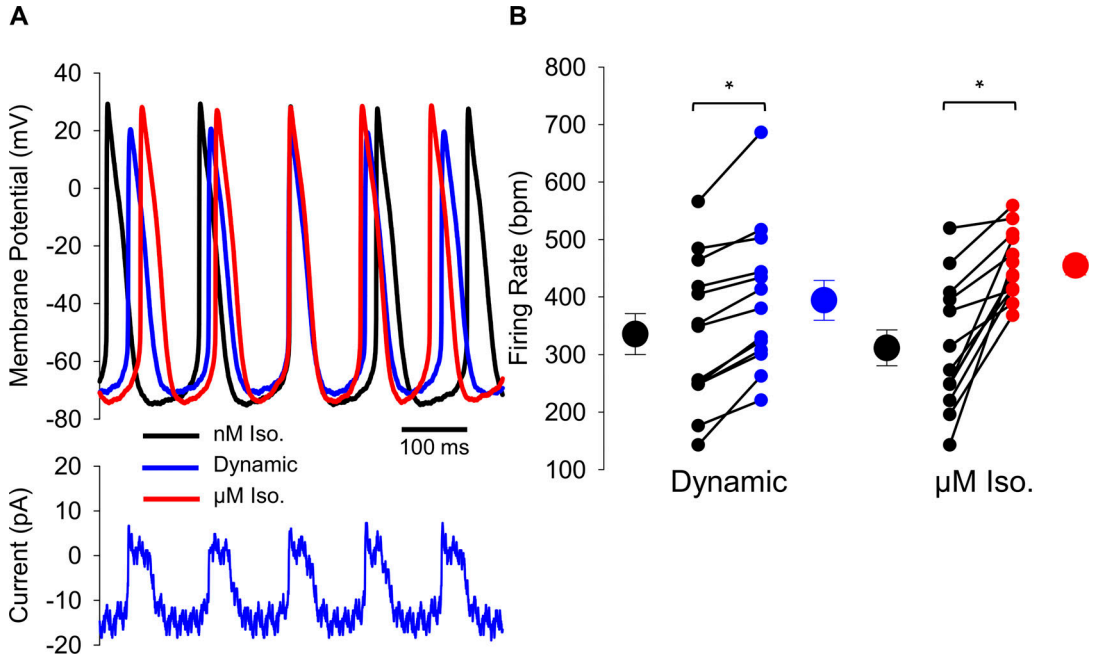

Figure 6. **Cell-scaled dynamic clamp shows βAR stimulation of I_f accounts for 36% of the increase in AP firing rate. (A)** Top: Representative sinoatrial APs from one cell in 1 nM Iso with no current injection (black), in 1 nM Iso with dynamic injection of βAR-stimulated I_f (blue), and in 1 μM Iso with no current injection (red). Bottom: Dynamic current injection (blue) during the APs recorded during dynamic clamp. **(B)** Average (±SEM) firing rate of cells in 1 nM Iso before (black) and after cell-scaled dynamic injection of βAR stimulated I_f (blue) or perfusion of 1 μM Iso (red). Individual recordings are shown as small circles (n = 13 for all cases). Control AP firing rates immediately preceding the dynamic $I_{f\text{-}Iso}$ addition and perfusion of 1 μM Iso did not differ significantly (P = 0.7432).

one hand, the slow rate of activation and hyperpolarized voltage-dependence of I_f seemingly preclude appreciable activation of I_f during the sinoatrial AP, even when βARs are stimulated (Lakatta and DiFrancesco, 2009). On the other hand, an essential role for I_f in cardiac pacemaking is clearly indicated by slower heart rates and sinus arrhythmias in response to I_f blockers and HCN4 mutations (Stieber et al., 2003; Herrmann et al., 2007; Hoesl et al., 2008; Harzheim et al., 2008; Alig et al., 2009; Baruscotti et al., 2011; Bucchi et al., 2012; Mesirca et al., 2014; Fenske et al., 2020). Our recent work using the AP-clamp technique helps to resolve this paradox by showing that I_f is constitutively active throughout the duration of the sinoatrial AP. This persistent activation allows I_f to conduct >50% of the net inward charge movement during the AP under control conditions, despite its low fractional open probability (Peters et al., 2021).

Importantly, our previous study also demonstrated that βAR stimulation increases the fraction of net inward charge movement conducted by I_f to 93% of the total (Peters et al., 2021), strongly suggesting that I_f contributes substantively to the fight-or-flight response in SAMs. A role for I_f in the βAR-mediated increase in sinoatrial AP firing rate has been postulated since the earliest description of I_f showed that adrenaline potentiates the current (Brown et al., 1979). Yet little direct data exist to support a role for I_f in the increase in AP firing rate, owing in part to the difficulty of isolating the effects of a single current in a complex interrelated system.

A number of studies through the years have used I_f blockers and mice bearing mutations in HCN4 to probe the role of I_f in the fight-or-flight response. Interpretation of such results is problematic for a number of reasons. In the case of blockers such as Cs^+ or ivabradine, incomplete or voltage-dependent block of I_f at commonly used concentrations (DiFrancesco, 1982; Bucchi et al., 2002; Peters et al., 2021) and off-target block of other currents (Lees-Miller et al., 2003; Haechl et al., 2019; Peters et al., 2021) can confound estimates of the contribution of I_f (Leitch et al., 1993; Cai et al., 1995; Du et al., 2004; Sosunov and Anyukhovsky, 2012).

In the case of mice with global or conditional knockout of HCN4 or with mutations that prevent cAMP from binding to the channels, interpretation is challenging because while these manipulations consistently cause lower or irregular resting and maximal heart rates in animals and spontaneous AP firing rates in isolated SAMs, they do not prevent a βAR-mediated increase in pacemaker activity from the slower baseline rates (Stieber et al., 2003; Herrmann et al., 2007; Hoesl et al., 2008; Harzheim et al., 2008; Baruscotti et al., 2011; Alig et al., 2009; Mesirca et al., 2014; Fenske et al., 2020).

It has been suggested that βAR-mediated increases in heart rate or firing rate from lower baseline levels exclude a role for I_f in the fight-or-flight response in SAMs (Zhang and Vassalle, 2003; Lakatta and DiFrancesco, 2009; Alig et al., 2009; Mesirca et al., 2014; Fenske et al., 2020; Hennis et al., 2021). However, this argument assumes that firing rate acceleration in a cell firing 200 AP/min and a cell firing 400 AP/min require a similar amount of depolarizing current. This is clearly not the case: the shorter diastolic interval in faster cells requires a larger depolarizing current to affect

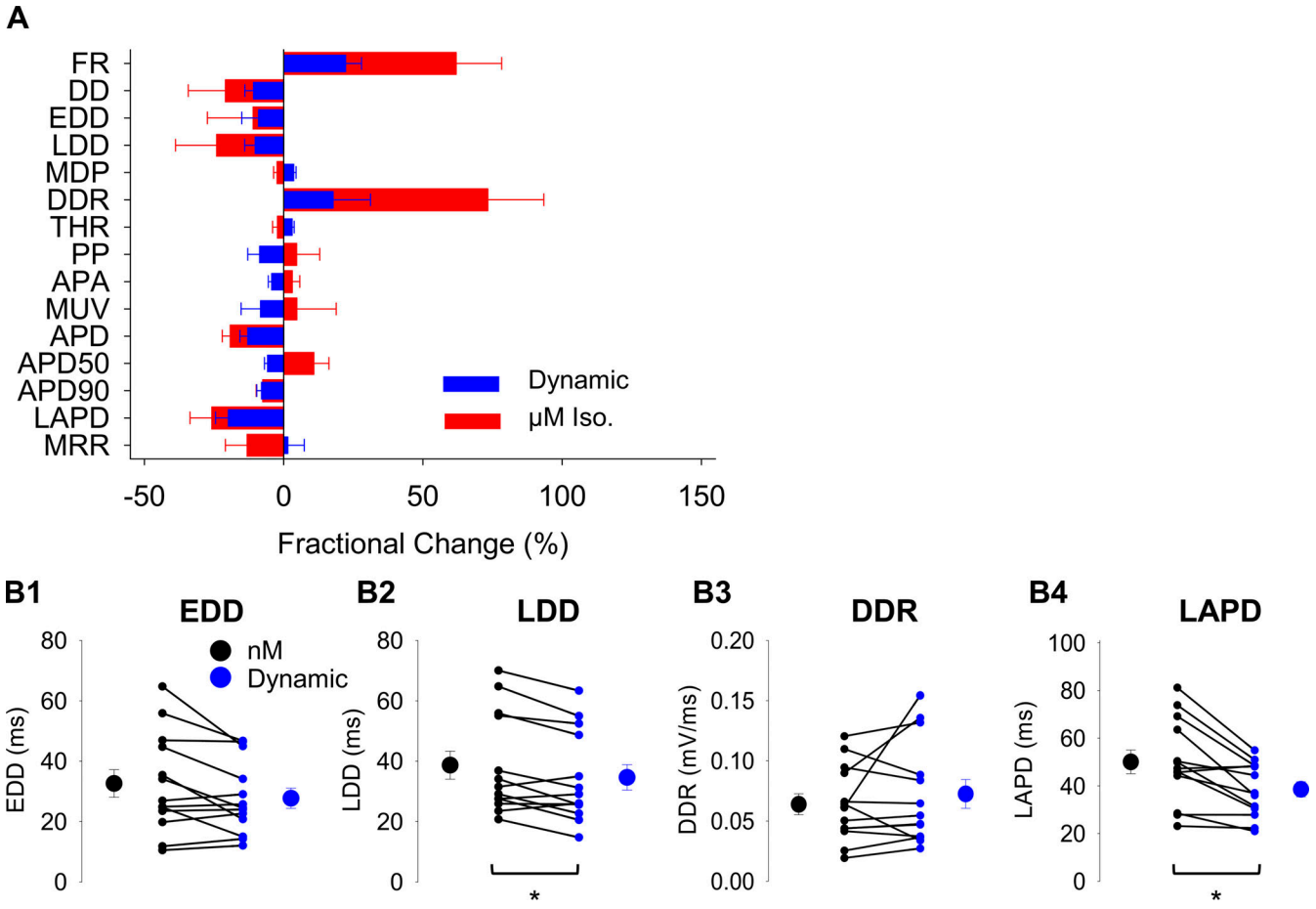

Figure 7. **βAR stimulation of I_f significantly shortens LAPD and DD. (A)** Average (±SE) fractional change (%) in sinoatrial AP firing rate and waveform parameters with perfusion of 1 µM Iso (red) or dynamic injection of βAR stimulated I_f (blue) compared to recordings in 1 nM Iso. **(B1–B4)** Average (+SEM) waveform parameters (EDD, LDD, DDR, LAPD) of cells in 1 nM Iso before (black) and after cell-scaled dynamic injection of βAR stimulated I_f (blue). Individual recordings are shown as small circles (n = 13 for all cases). Details of statistical tests can be found in Table S2.

the same change in membrane potential to reach threshold. Thus, in slower cells—such as when I_f is reduced by blockers or mutations—βAR stimulation may have sufficient time to produce a "normal" increase in firing rate via additional pathways, whereas in faster cells the same incomplete stimulation would produce a smaller increase in firing rate. Indeed, analysis of all the APs recorded in the present study show that a larger βAR-mediated increase in AP firing rate is correlated with a larger increase in DDR (Fig. 3 A4). Moreover, analysis of cells binned by firing rate reveals that a 118 AP/min increase in mean firing rate in faster cells (from 338 to 456 AP/min, n = 54) requires that the DDR increase by 0.044 mV/ms, which is about three times the DDR increase associated with a similar magnitude firing rate increase (121 AP/min) in slower cells (217 to 338 AP/min, n = 54; corresponding to a DDR increase of 0.015 mV/ms; Table S3).

Taken together, previous studies all consistently demonstrate a residual fight-or-flight increase in pacemaking in the absence of I_f, clearly indicating that I_f alone is insufficient to produce the full response. However, these results do not preclude a contribution of I_f to the response given the reduction in basal rates.

βAR stimulation of I_f alone accounts for >40% of the increase in AP firing rate

To quantitatively determine the role that βAR stimulation of I_f plays in firing rate acceleration in SAMs, we used the dynamic clamp technique with models parameterized to I_f recorded from SAMs under identical conditions and validated by AP-clamp experiments (Peters et al., 2021). The dynamic clamp currents in our experiments were scaled to the endogenous I_f directly measured in each cell (Fig. S2). While a prior study used dynamic clamp in rabbit SAMs to investigate the role of βAR stimulation of I_f in that system, the I_f conductance was scaled indirectly, through a calibration curve constructed by relating I_f amplitude to firing rate in a mathematical model of the sinoatrial AP (Severi et al., 2012; Ravagli et al., 2016). Unfortunately, this scaling paradigm is recursive, as it assumes that differences in firing rate are exclusively due to changes in the I_f amplitude. Moreover, the I_f models used in the prior study only accounted for βAR-stimulated shifts in the voltage-dependence I_f but not the changes in kinetics, despite the fact that βAR speeding of activation and slowing of deactivation of I_f are fundamental to its role in pacemaking (Peters et al., 2021). Despite these differences in approach and system, the results of the two dynamic clamp

studies are comparable, with our data showing that βAR-stimulated I_f drives 41% of the increase in AP firing rate in mouse SAMs (Fig. 6) similar to the ~38% fraction in rabbit SAMs (Ravagli et al., 2016).

Our study further leveraged automated AP waveform analysis to additionally demonstrate that βAR modulation of I_f accounts for 60% of the shortening between APs, including 50% of the DD shortening and 80% of the LAPD shortening that occur with βAR stimulation (Fig. 7). Since these parameters are primary determinants of the βAR increase in AP firing rate determined by correlation analysis and machine learning (Fig. 3), they further highlight the importance of I_f in the fight-or-flight response in SAMs. We are not aware of any prior studies that quantified the duration of the LAPD—defined as the time from when the threshold potential is reached during the repolarization until the subsequent maximum diastolic potential (Table 1 and Fig. S3)—despite the fact that it accounts for nearly 25% of the total cycle length and a third of the time spent in diastole. The prominent role for I_f during this phase of the AP is consistent with our recent finding that I_f remains active throughout the AP (Peters et al., 2021) and the βAR-stimulated increase in I_f is uniquely well suited to act on LAPD when other depolarizing currents are not predicted to be active.

Other currents must contribute to the fight-or-flight response in SAMs

Not only does I_f not account for the total increase in AP firing rate upon βAR stimulation in SAMs, but it also does not account for the changes in the AP waveform. Equally informative as the AP parameters that change upon I_f injection are those that do not change. Compared to Iso stimulation, injection of βAR-stimulated component of I_f alone produces opposite effects on the MDP, THR, PP, APA, MUV, APD_{50}, and MRR (Fig. 7 A). The opposite effects of Iso and $I_{f\text{-}Iso}$ on the MDP indicate that sympathetic stimulation must also increase an outward current that is active during the diastolic depolarization, possibly a voltage-gated or calcium-sensitive potassium channel (Torrente et al., 2017; Lai et al., 2014). Similarly, Iso must stimulate an inward current—such as $Na_v1.1$ or $Ca_v1.2$ (Hagiwara et al., 1988; Lei et al., 2004)—during the AP upstroke to depolarize the APA and the MUV. Furthermore, it is clear that inward current through NCX also contributes to the fight-or-flight response in SAMs and further shortening of DD (Lakatta et al., 2010; Gao et al., 2013).

Conclusions

While our direct measurements provide a uniquely quantitative resolution of the contribution of I_f to βAR-mediated increases in AP firing rate in SAMs, they also clearly indicate that other currents are required. Given the fundamental importance of the fight-or-flight increase in heart rate in mammals, it is reassuring to know that redundant mechanisms are involved. As noted by Lipsius and Bers nearly two decades ago, "it is … prudent to adopt a more balanced integrative view of the cardiac pacemaker, and acknowledge the real interplay of many factors" (Lipsius and Bers, 2003). The challenge for future studies is to resolve the coordinated and interrelated responses of multiple molecular processes.

Acknowledgments

Jeanne M. Nerbonne served as editor.

This work was funded by National Institutes of Health grants R01 HL088427 to C. Proenza, R01HL131517, R01HL141214, and P01HL141084; the Stimulating Peripheral Activity to Relieve Conditions Grants OT2OD026580 to E. Grandi and R00HL138160 to S. Morotti; and by postdoctoral fellowships from the American Heart Association (19POST34380777 and 830889) to C.H. Peters. The Optogenetics and Neural Engineering (ONE) Core at the University of Colorado School of Medicine provided engineering support for this research. The ONE Core is part of the NeuroTechnology Center, funded in part by the School of Medicine and by the National Institute of Neurological Disorders and Stroke of the National Institutes of Health under award number P30NS048154. Dr. Debashis Ghosh (University of Colorado, Anschutz Medical Campus, Department of Biostatistics and Informatics) provided consulting on machine learning analysis for this paper.

The authors declare no competing financial interests.

Author contributions: C.H. Peters—conceptualization, formal analysis, investigation, methodology, validation, visualization, writing—original draft, writing—review & editing. C. Rickert—conceptualization, data curation, formal analysis, investigation, methodology, software, validation, writing—review & editing. S. Morotti—formal analysis, software, validation, writing—review & editing. E. Grandi—formal analysis, software, validation, writing—review & editing. K.A. Aronow—methodology, validation, writing—review & editing. K. Beam—conceptualization, methodology, validation, writing—review & editing. C. Proenza—conceptualization, data curation, funding acquisition, project administration, resources, supervision, validation, visualization, writing—review & editing.

Submitted: 12 May 2022
Revised: 22 August 2022
Accepted: 4 October 2022

References

Alig, J., L. Marger, P. Mesirca, H. Ehmke, M.E. Mangoni, and D. Isbrandt. 2009. Control of heart rate by cAMP sensitivity of HCN channels. *Proc. Natl. Acad. Sci. USA.* 106:12189–12194. https://doi.org/10.1073/pnas.0810332106

Baruscotti, M., A. Bucchi, C. Viscomi, G. Mandelli, G. Consalez, T. Gnecchi-Rusconi, N. Montano, K.R. Casali, S. Micheloni, A. Barbuti, and D. DiFrancesco. 2011. Deep bradycardia and heart block caused by inducible cardiac-specific knockout of the pacemaker channel gene Hcn4. *Proc. Natl. Acad. Sci. USA.* 108:1705–1710. https://doi.org/10.1073/pnas.1010122108

Boyett, M.R., H. Honjo, and I. Kodama. 2000. The sinoatrial node, a heterogeneous pacemaker structure. *Cardiovasc. Res.* 47:658–687. https://doi.org/10.1016/S0008-6363(00)00135-8

Breiman, L. 2001. Random forests. *Mach. Learn.* 45:5–32. https://doi.org/10.1023/A:1010933404324

Brown, H.F., D. Difrancesco, and S.J. Noble. 1979. How does adrenaline accelerate the heart? *Nature.* 280:235–236. https://doi.org/10.1038/280235a0

Bucchi, A., A. Barbuti, D. Difrancesco, and M. Baruscotti. 2012. Funny current and cardiac rhythm: Insights from HCN knockout and transgenic mouse models. *Front. Physiol.* 3:240. https://doi.org/10.3389/fphys.2012.00240

Bucchi, A., M. Baruscotti, and D. DiFrancesco. 2002. Current-dependent block of rabbit sino-atrial node if channels by ivabradine. *J. Gen. Physiol.* 120:1–13. https://doi.org/10.1085/jgp.20028593

Bucchi, A., M. Baruscotti, R.B. Robinson, and D. DiFrancesco. 2007. Modulation of rate by autonomic agonists in SAN cells involves changes in diastolic depolarization and the pacemaker current. *J. Mol. Cell. Cardiol.* 43:39–48. https://doi.org/10.1016/j.yjmcc.2007.04.017

Cai, Q., M. Lei, and H. Brown. 1995. Responses of guinea-pig SA node/atria to acetylcholine and adrenaline in the presence of blockers of if and IK, ACh. *J. Physiol.* 483:21P

Desai, N., R. Gray, and D. Johnston. 2017. Microprocessor-based dynamic clamp. *eNeuro.* 4:ENEURO.0250-17.2017. https://doi.org/10.1523/ENEURO.0250-17.2017

DiFrancesco, D. 1982. Block and activation of the pace-maker channel in calf purkinje fibres: Effects of potassium, caesium and rubidium. *J. Physiol.* 329:485–507. https://doi.org/10.1113/jphysiol.1982.sp014315

DiFrancesco, D. 2010. The role of the funny current in pacemaker activity. *Circ. Res.* 106:434–446. https://doi.org/10.1161/CIRCRESAHA.109.208041

DiFrancesco, D., A. Ferroni, M. Mazzanti, and C. Tromba. 1986. Properties of the hyperpolarizing-activated current (if) in cells isolated from the rabbit sino-atrial node. *J. Physiol.* 377:61–88. https://doi.org/10.1113/jphysiol.1986.sp016177

Du, X.-J., X. Feng, X.-M. Gao, T.P. Tan, H. Kiriazis, and A.M. Dart. 2004. If channel inhibitor ivabradine lowers heart rate in mice with enhanced sympathoadrenergic activities. *Br. J. Pharmacol.* 142:107–112. https://doi.org/10.1038/sj.bjp.0705696

Fenske, S., K. Hennis, R.D. Rötzer, V.F. Brox, E. Becirovic, A. Scharr, C. Gruner, T. Ziegler, V. Mehlfeld, J. Brennan, et al. 2020. cAMP-dependent regulation of HCN4 controls the tonic entrainment process in sinoatrial node pacemaker cells. *Nat. Commun.* 11:5555. https://doi.org/10.1038/s41467-020-19304-9

Gao, Z., T.P. Rasmussen, Y. Li, W. Kutschke, O.M. Koval, Y. Wu, Y. Wu, D.D. Hall, M.l. A. Joiner, X.-Q. Wu, et al. 2013. Genetic inhibition of Na^+-Ca^{2+} exchanger current disables fight or flight sinoatrial node activity without affecting resting heart rate. *Circ. Res.* 112:309–317. https://doi.org/10.1161/CIRCRESAHA.111.300193

Giles, W.R., and Y. Imaizumi. 1988. Comparison of potassium currents in rabbit atrial and ventricular cells. *J. Physiol.* 405:123–145. https://doi.org/10.1113/jphysiol.1988.sp017325

Haechl, N., J. Ebner, K. Hilber, H. Todt, and X. Koenig. 2019. Pharmacological profile of the bradycardic agent ivabradine on human cardiac ion channels. *Cell. Physiol. Biochem.* 53:36–48. https://doi.org/10.33594/000000119

Hagiwara, N., H. Irisawa, and M. Kameyama. 1988. Contribution of two types of calcium currents to the pacemaker potentials of rabbit sino-atrial node cells. *J. Physiol.* 395:233–253. https://doi.org/10.1113/jphysiol.1988.sp016916

Harzheim, D., K.H. Pfeiffer, L. Fabritz, E. Kremmer, T. Buch, A. Waisman, P. Kirchhof, U.B. Kaupp, and R. Seifert. 2008. Cardiac pacemaker function of HCN4 channels in mice is confined to embryonic development and requires cyclic AMP. *EMBO J.* 27:692–703. https://doi.org/10.1038/emboj.2008.3

Hennis, K., R.D. Rötzer, C. Piantoni, M. Biel, C. Wahl-Schott, and S. Fenske. 2021. Speeding up the heart? Traditional and new perspectives on HCN4 function. *Front. Physiol.* 12:669029. https://doi.org/10.3389/fphys.2021.669029

Herrmann, S., J. Stieber, G. Stöckl, F. Hofmann, and A. Ludwig. 2007. HCN4 provides a "depolarization reserve" and is not required for heart rate acceleration in mice. *EMBO J.* 26:4423–4432. https://doi.org/10.1038/sj.emboj.7601868

Hoesl, E., J. Stieber, S. Herrmann, S. Feil, E. Tybl, F. Hofmann, R. Feil, and A. Ludwig. 2008. Tamoxifen-inducible gene deletion in the cardiac conduction system. *J. Mol. Cell. Cardiol.* 45:62–69. https://doi.org/10.1016/j.yjmcc.2008.04.008

Keith, A., and M. Flack. 1907. The form and nature of the muscular connections between the primary divisions of the vertebrate heart. *J. Anat. Physiol.* 41:172–189

Lai, M.H., Y. Wu, Z. Gao, M.E. Anderson, J.E. Dalziel, and A.L. Meredith. 2014. BK channels regulate sinoatrial node firing rate and cardiac pacing in vivo. *Am. J. Physiol. Heart Circ. Physiol.* 307:H1327–H1338. https://doi.org/10.1152/ajpheart.00354.2014

Lakatta, E.G., and D. DiFrancesco. 2009. JMCC point-counterpoint. *J. Mol. Cell. Cardiol.* 47:157–170. https://doi.org/10.1016/j.yjmcc.2009.03.022

Lakatta, E.G., V.A. Maltsev, and T.M. Vinogradova. 2010. A coupled SYSTEM of intracellular Ca^{2+} clocks and surface membrane voltage clocks controls the timekeeping mechanism of the heart's pacemaker. *Circ. Res.* 106:659–673. https://doi.org/10.1161/CIRCRESAHA.109.206078

Larson, E.D., J.R.S. Clair, W.A. Sumner, R.A. Bannister, and C. Proenza. 2013. Depressed pacemaker activity of sinoatrial node myocytes contributes to the age-dependent decline in maximum heart rate. *Proc. Natl. Acad. Sci. USA.* 110:18011–18016. https://doi.org/10.1073/pnas.1308477110

Lees-Miller, J.P., J. Guo, J.R. Somers, D.E. Roach, R.S. Sheldon, D.E. Rancourt, and H.J. Duff. 2003. Selective knockout of mouse ERG1 B Potassium channel eliminates IKr in adult ventricular myocytes and elicits episodes of abrupt sinus bradycardia. *Mol. Cell. Biol.* 23:1856–1862. https://doi.org/10.1128/MCB.23.6.1856-1862.2003

Lei, M., S.A. Jones, J. Liu, M.K. Lancaster, S.S.-M. Fung, H. Dobrzynski, P. Camelliti, S.K.G. Maier, D. Noble, and M.R. Boyett. 2004. Requirement of neuronal- and cardiac-type sodium channels for murine sinoatrial node pacemaking. *J. Physiol.* 559:835–848. https://doi.org/10.1113/jphysiol.2004.068643

Leitch, S.P., H.F. Brown, and D.J. Paterson. 1993. Effect of caesium and β-adrenergic agonists on the rate of spontaneous activity in an isolated rabbit sino-atrial node preparation. *J. Physiol.* 459:86P

Liao, Z., D. Lockhead, E.D. Larson, and C. Proenza. 2010. Phosphorylation and modulation of hyperpolarization-activated HCN4 channels by protein kinase A in the mouse sinoatrial node. *J. Gen. Physiol.* 136:247–258. https://doi.org/10.1085/jgp.201010488

Lipsius, S.L., and D.M. Bers. 2003. Cardiac pacemaking: I_f vs. Ca^{2+}, is it really that simple? *J. Mol. Cell. Cardiol.* 35:891–893. https://doi.org/10.1016/S0022-2828(03)00184-6

Lucot, J.B., N. Jackson, I. Bernatova, and M. Morris. 2005. Measurement of plasma catecholamines in small samples from mice. *J. Pharmacol. Toxicol. Methods.* 52:274–277. https://doi.org/10.1016/j.vascn.2004.11.004

Maltsev, A.V., M.D. Stern, E.G. Lakatta, and V.A. Maltsev. 2022. Functional heterogeneity of cell populations increases robustness of pacemaker function in a numerical model of the sinoatrial node tissue. *Front. Physiol.* 13:845634. https://doi.org/10.3389/fphys.2022.845634

Mesirca, P., J. Alig, A.G. Torrente, J.C. Müller, L. Marger, A. Rollin, C. Marquilly, A. Vincent, S. Dubel, I. Bidaud, et al. 2014. Cardiac arrhythmia induced by genetic silencing of "funny" (f) channels is rescued by GIRK4 inactivation. *Nat. Commun.* 5:4664. https://doi.org/10.1038/ncomms5664

Messan, F., A. Tito, P. Gouthon, K.B. Nouatin, I.B. Nigan, A.S. Blagbo, J. Lounana, and J. Medelli. 2017. Comparison of catecholamine values before and after exercise-induced bronchospasm in professional cyclists. *Tanaffos.* 16:136–143

Milano, A., A.M.C. Vermeer, E.M. Lodder, J. Barc, A.O. Verkerk, A.V. Postma, I.A.C. van der Bilt, M.J.H. Baars, P.L. van Haelst, K. Caliskan, et al. 2014. HCN4 mutations in multiple families with bradycardia and left ventricular noncompaction cardiomyopathy. *J. Am. Coll. Cardiol.* 64:745–756. https://doi.org/10.1016/j.jacc.2014.05.045

Moosmang, S., M. Biel, F. Hofmann, and A. Ludwig. 1999. Differential distribution of four hyperpolarization-activated cation channels in mouse brain. *Biol. Chem.* 380:975–980. https://doi.org/10.1515/BC.1999.121

Pedregosa, F., G. Varoquaux, A. Gramfort, V. Michel, B. Thirion, O. Grisel, M. Blondel, P. Prettenhofer, R. Weiss, V. Dubourg, et al. 2011. Scikit-learn: Machine learning in Python. *J. Mach. Learn. Res.* 12:2825–2830

Peters, C.H., P.W. Liu, S. Morotti, S.C. Gantz, E. Grandi, B.P. Bean, and C. Proenza. 2021. Bidirectional flow of the funny current (If) during the pacemaking cycle in murine sinoatrial node myocytes. *Proc. Natl. Acad. Sci. USA.* 118:e2104668118. https://doi.org/10.1073/pnas.2104668118

Pichavaram, P., W. Yin, K.W. Evanson, J.H. Jaggar, and S. Mancarella. 2018. Elevated plasma catecholamines functionally compensate for the reduced myogenic tone in smooth muscle STIM1 knockout mice but with deleterious cardiac effects. *Cardiovasc. Res.* 114:668–678. https://doi.org/10.1093/cvr/cvy015

Protze, S.I., J. Liu, U. Nussinovitch, L. Ohana, P.H. Backx, L. Gepstein, and G.M. Keller. 2017. Sinoatrial node cardiomyocytes derived from human pluripotent cells function as a biological pacemaker. *Nat. Biotechnol.* 35:56–68. https://doi.org/10.1038/nbt.3745

Ravagli, E., A. Bucchi, C. Bartolucci, M. Paina, M. Baruscotti, D. DiFrancesco, and S. Severi. 2016. Cell-specific Dynamic Clamp analysis of the role of

funny If current in cardiac pacemaking. *Prog. Biophys. Mol. Biol.* 120: 50–66. https://doi.org/10.1016/j.pbiomolbio.2015.12.004

Rickert, C., and C. Proenza. 2017. ParamAP: Standardized parameterization of sinoatrial node myocyte action potentials. *Biophys. J.* 113:765–769. https://doi.org/10.1016/j.bpj.2017.07.001

Rickert, C., and C. Proenza. 2019a. pyClamp: A live graphical user interface for the dyClamp sketch. *Zenodo*. https://doi.org/10.5281/zenodo.2825278

Rickert, C., and C. Proenza. 2019b. dyClamp: A real-time dynamic clamp sketch for the pyClamp interface. *Zenodo*. https://doi.org/10.5281/zenodo.2824830

Rickert, C., and C. Proenza. 2021. christianrickert/ParamAP: Third release. *Zenodo*. https://doi.org/10.5281/zenodo.5250113

Severi, S., M. Fantini, L.A. Charawi, and D. DiFrancesco. 2012. An updated computational model of rabbit sinoatrial action potential to investigate the mechanisms of heart rate modulation. *J. Physiol.* 590:4483–4499. https://doi.org/10.1113/jphysiol.2012.229435

Sharpe, E.J., J.R.S. Clair, and C. Proenza. 2016. Methods for the isolation, culture, and functional characterization of sinoatrial node myocytes from adult mice. *J. Vis. Exp.*:54555. https://doi.org/10.3791/54555

Sharpe, E.J., E.D. Larson, and C. Proenza. 2017. Cyclic AMP reverses the effects of aging on pacemaker activity and if in sinoatrial node myocytes. *J. Gen. Physiol.* 149149:237237–247247. https://doi.org/10.1085/jgp.201611674

Sosunov, E.A., and E.P. Anyukhovsky. 2012. Differential effects of ivabradine and ryanodine on pacemaker activity in canine sinus node and purkinje fibers. *J. Cardiovas. Electrophysiol.* 23:650–655. https://doi.org/10.1111/j.1540-8167.2011.02285.x

Stieber, J., S. Herrmann, S. Feil, J. Löster, R. Feil, M. Biel, F. Hofmann, and A. Ludwig. 2003. The hyperpolarization-activated channel HCN4 is required for the generation of pacemaker action potentials in the embryonic heart. *Proc. Natl. Acad. Sci. USA*. 100:15235–15240. https://doi.org/10.1073/pnas.2434235100

Swedberg, K., M. Komajda, M. Böhm, J.S. Borer, I. Ford, A. Dubost-Brama, G. Lerebours, L. Tavazzi, and SHIFT Investigators. 2010. Ivabradine and outcomes in chronic heart failure (SHIFT): A randomised placebo-controlled study. *Lancet*. 376:875–885. https://doi.org/10.1016/S0140-6736(10)61198-1

Torrente, A.G., R. Zhang, H. Wang, A. Zaini, B. Kim, X. Yue, K.D. Philipson, and J.I. Goldhaber. 2017. Contribution of small conductance K^+ channels to sinoatrial node pacemaker activity: Insights from atrial-specific Na^+/Ca^{2+} exchange knockout mice. *J. Physiol.* 595:3847–3865. https://doi.org/10.1113/JP274249

Verkerk, A.O., G.S.C. Geuzebroek, M.W. Veldkamp, and R. Wilders. 2012. Effects of acetylcholine and noradrenalin on action potentials of isolated rabbit sinoatrial and atrial myocytes. *Front. Physiol.* 3:174. https://doi.org/10.3389/fphys.2012.00174

Zhang, H., and M. Vassalle. 2003. Mechanisms of adrenergic control of sinoatrial node discharge. *J. Biomed. Sci.* 10:179–192. https://doi.org/10.1007/BF02256053

Supplemental material

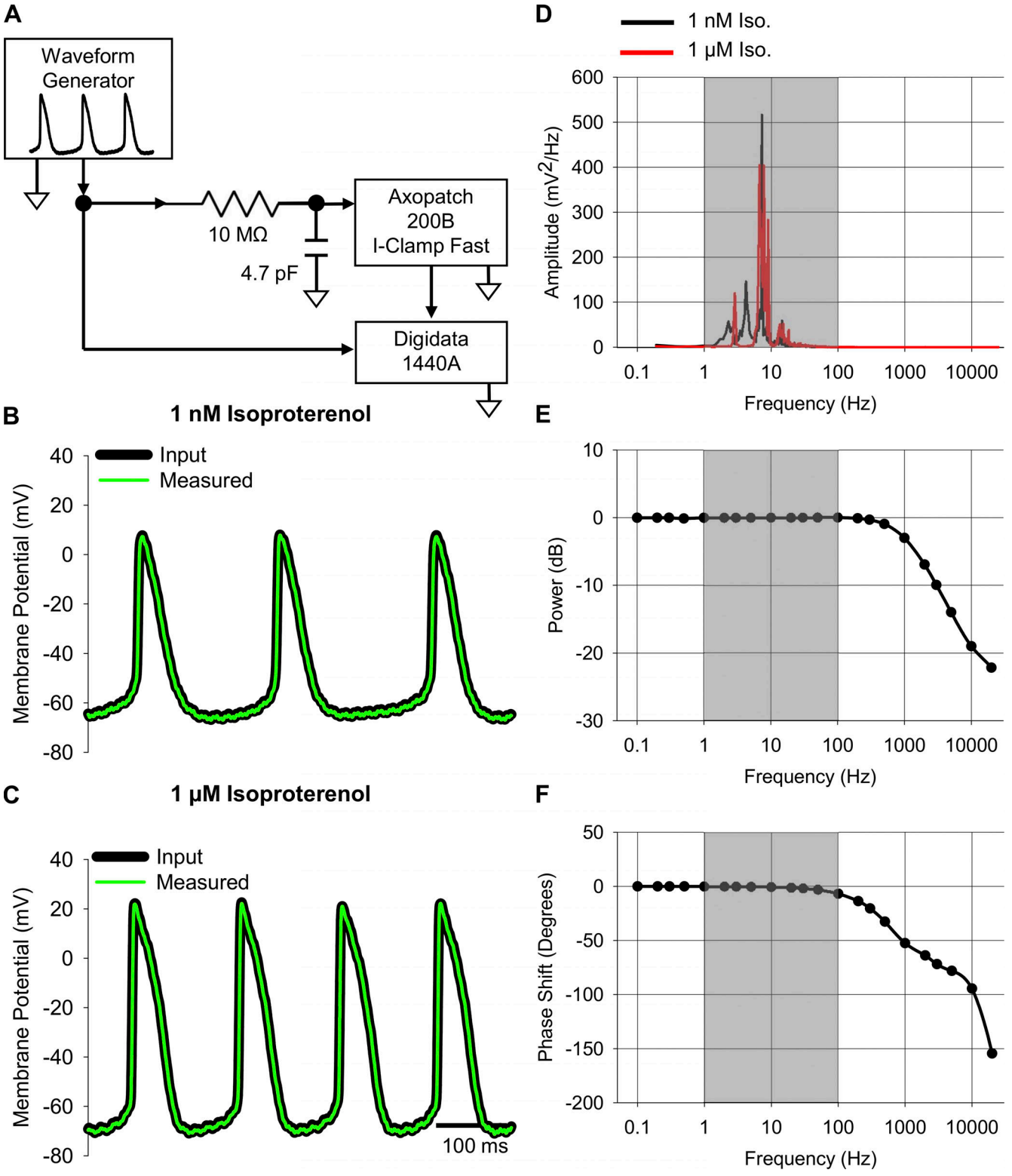

Figure S1. **Axon Axopatch 200B validation. (A)** Schematic of the circuit used to test the response of the Axopatch 200B amplifier in response to the voltage output from a waveform generator. The signal from the waveform generator was split to allow direct comparison of the amplifier output to the original signal. **(B and C)** Representative sinoatrial APs originally recorded in 1 nM (B) and 1 µM Iso (C) as measured through the model circuit by the Axopatch 200B (green) compared to the original signal (black). **(D)** Average frequency content of sinoatrial APs recorded in 1 nM (black, *n* = 13) and 1 µM Iso (red, *n* = 13) determined by fast Fourier transform. **(E and F)** Bode plots showing the differences in magnitude (E) and phase (F) for 100 mV sine waves of different frequencies as recorded by the Axopatch 200B compared to the original signals. Gray boxes in D–F indicate the frequency range (1–100 Hz) that contains >99% of the sinoatrial AP signal.

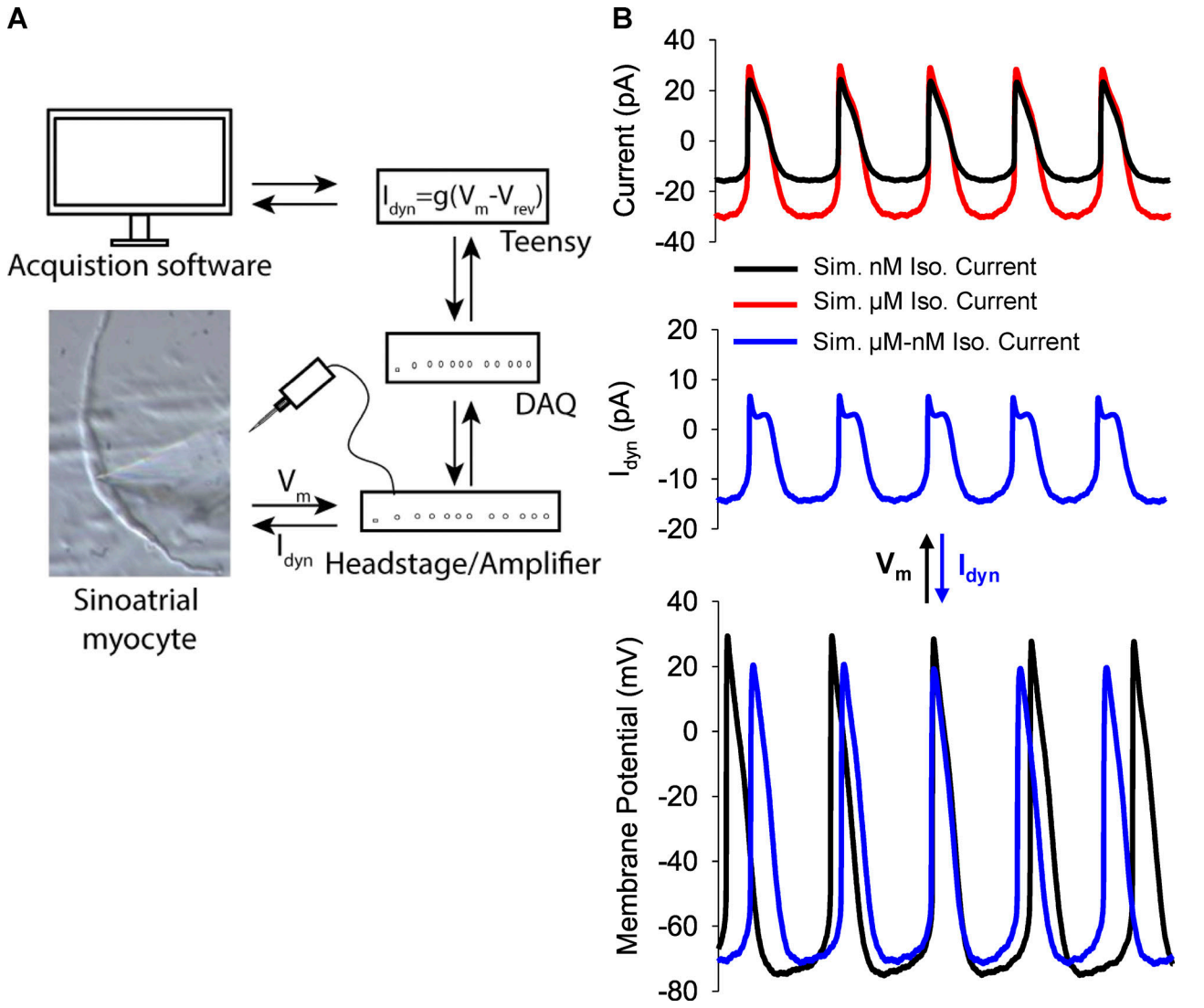

Figure S2. **Dynamic clamp approach. (A)** Schematic of the dynamic clamp technique. **(B)** Membrane voltages recorded from a patch-clamped SAM are used by a Teensy microprocessor to simulate currents using models of I_f in 1 nM and 1 µM Iso (top right). The calculated dynamic clamp current (I_{dyn}), corresponding to the Iso-sensitive component of I_f (middle right), is then injected back into the SAM in a fast feedback loop, and the resulting changes to AP firing are recorded (bottom right).

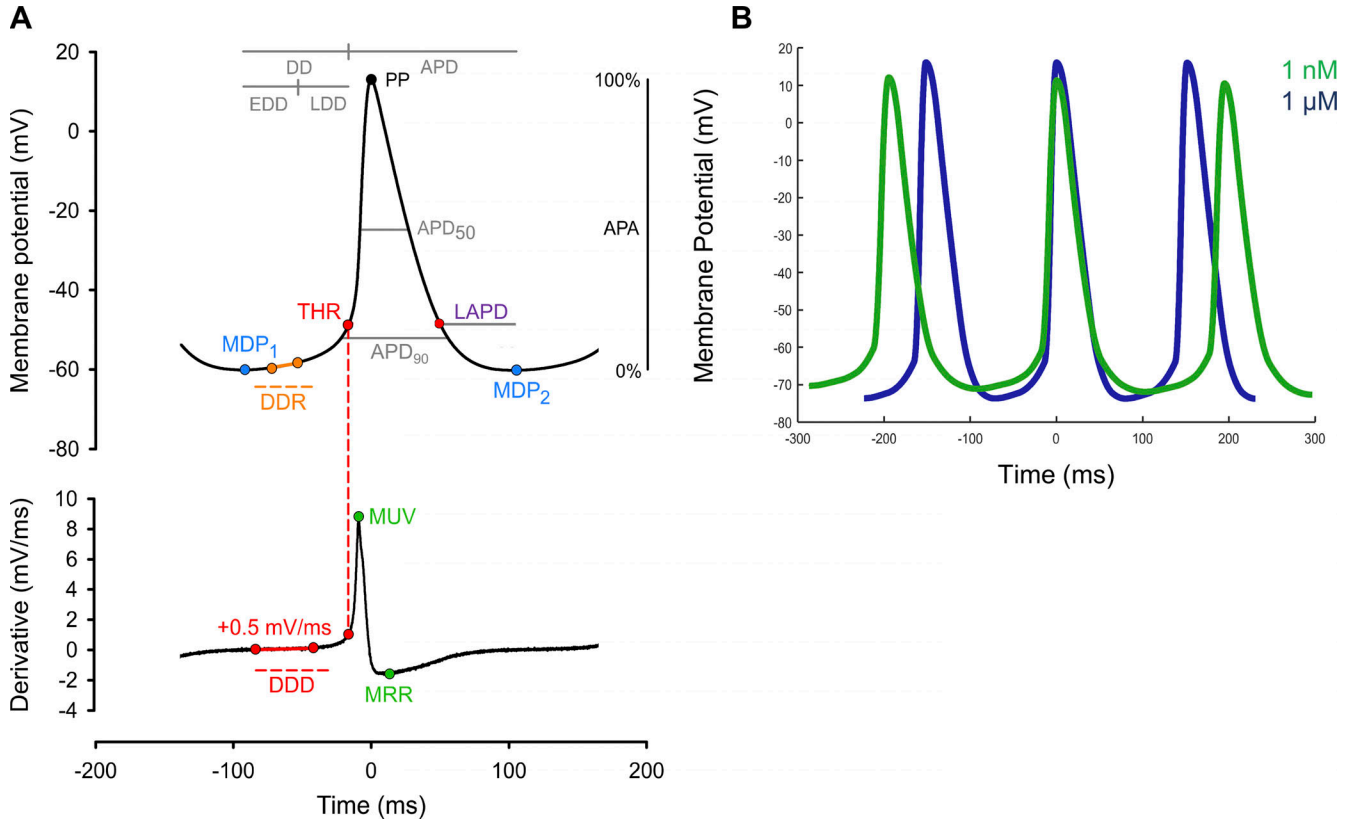

Figure S3. **ParamAP automates determination of sinoatrial node AP waveform parameters and fully parameterizes the AP. (A)** Schematic illustration of ParamAP waveform parameters, including the new parameter LAPD (purple). Figure adapted from Rickert and Proenza (2017). **(B)** Sinoatrial AP waveforms modeled by line segments representing average waveform parameters determined by ParamAP in 1 nM or 1 µM Iso indicate that ParamAP adequately parameterizes the sinoatrial AP.

Provided online are four tables. Table S1 shows Pearson correlation coefficients between firing rate and waveform parameters in 1 nM and 1 µM Iso. Table S2 shows dynamic clamp changes in AP firing rate and AP waveform. Table S3 shows DDR in cells binned by firing rate. Table S4 shows errors in sinoatrial AP waveform parameters introduced by the Axopatch 200B amplifier.